Aus der
Universitätsklinik für Urologie Tübingen

A novel needle-free WaterJet technique for injecting porcine muscle-derived cells into the urethra

Inaugural-Dissertation
zur Erlangung des Doktorgrades
der Medizin

der Medizinischen Fakultät
der Eberhard-Karls-Universität
zu Tübingen

vorgelegt von

Geng, Ruizhi

2023

Dekan: Professor Dr. B. Pichler

1. Berichterstatter: Professor Dr. W.K. Aicher
2. Berichterstatter: Professor Dr. T. Schäffer

Tag der Disputation: 22.12.2022

Table of Contents

List of Abbreviations

UI	Urinary incontinence
SUI	Stress urinary incontinence
ISD	Intrinsic sphincter deficiency
AUS	Artificial urinary sphincter
MSCs	Mesenchymal stromal cells
bmMSCs	Bone marrow MSCs
ADSCs	Adipose tissue−derived stromal cells
MDCs	Muscle−derived cells
WJ	WaterJet
WN	William's Needle
CS	Cadaveric sample
LA	Living animals
pMDCs	Porcine muscle−derived cells
UPP	Urethral wall pressure profiles
MUCP	Maximum urethral closure pressure
IVIS	In Vivo Imaging System
HE	Hematoxylin−eosin
DISIC	The distance between sphincter muscle and injected cells

List of Figures

List of Tables

1 Introduction

Millions of people experience urinary incontinence (UI), also called involuntary urination, defined as "any involuntary loss of urine that is a social or hygienic problem."[1]. UI may reduce the quality of life for patients as an embarrassing problem[2] and only 25% of people seek or get treatment[3]. Moreover, a higher incidence of depression was observed in patients with UI[4]. A range of 5% ~ 60% male patients suffered from UI after radical prostatectomy, the surgical treatment to prostate cancer which is the most frequently diagnosed type of cancer in men[5]. UI is more common in females than in males. Some studies reported that nearly 50% of adult women may be affected by this condition[2]. In china, UI affects up to 28.9% of the adult population, meaning 25.1% of men and 32.4% in women[6]. According to the recommendation by ICS, there are different types of urinary incontinence as stress urinary incontinence (SUI), urge, overflow, mixed and other types of incontinence[1].

Stress urinary incontinence, also called effort incontinence, is the involuntary leakage of urine during activities that increase the intra−abdominal pressure on the bladder associated with coughing, sneezing, laughing and physical exercise. As mentioned above, in men, SUI is the most common type after prostate surgery[7]. Similarly, in women, SUI is the common type accounting for 49% of the total UI[8]. Estimated 50% females under 65 years age suffered from SUI[9]. What's more important, it is considered to be largely underestimated or under reported, due to the fact that many SUI patients, which regarded it as a hidden handicap, would not search for help[10].

To investigate SUI, the anatomy and function of the bladder, and its outlet should be examined. The bladder can be divided into two parts: a body lying above the

ureteral orifices and a base consisting of the trigone and bladder neck. The bladder is involved primarily in compliant distension during gradual ureteral filling. With low pressure filling, the storage of urine occurs. Generation of efficient detrusor contraction causes voiding. The bladder outlet is composed of the bladder base, urethra, and striated urethral sphincter muscle (rhabdosphincter). In women, an anatomic smooth−muscle sphincter at the bladder neck is not obvious[11]. The proximal circular smooth muscle formed by type II fast twitch myofibers is responsible for the intermittent reflex and voluntary contractions at the bladder neck. The distal/external Ω−shaped striated sphincter formed by type I slow twitch myofibers is responsible for baseline tonic activity under partial voluntary control[12] Thus, urinary continence results from the combination of active muscle tone and passive anatomic coaptation.

The pathogenesis of SUI includes three most common responses: intrinsic sphincter deficiency (ISD), pelvic floor weakness, and urethral hypermobility[13, 14]. SUI can occur while the urethra keeps its normal position. ISD may be due to aging, hormonal changes, nerve injury during childbirth, pelvic surgery, and other factors. In this situation, the walls of the urethra simply are not able to create an effective seal. Although there is no specific test for ISD, it is now generally believed that many women with SUI have at least some degree of ISD. The urethral abnormality may be due to the other two causes. First, the urethra may be poorly supported, referred to as urethral hypermobility[15]. Loss of urethral support is frequently associated with loss of support for the other pelvic organs (prolapse), particularly the bladder[16].

At present, the treatment of SUI mainly includes conservative treatment and surgical treatment. Kegel exercise with biofeedback and electrical stimulation has been a first−line conservative measure to strengthen lower pelvic floor muscles[17, 18]. But only in patients with a high degree of compliance and taking up to 15−20

weeks of treatment, this method has a significant therapeutic effect[19]. Unsurprisingly, during the treatment process, the probability of patients giving up due to various reasons is very high, with a low proportion of patients who can restore complete function[20-22]. Bladder training, has to follow a fixed schedule to urinate. Electromagnetic therapy produces gentle, low induction impulses which help to stimulate and rejuvenate the cells in the body. Vaginal pessaries is a flexible device that is inserted into the vagina. It repositions and supports the urethra[23, 24]. Medical treatment has not been approved as effective and well−tolerated therapy. It therefore is not the preferred clinician's choice[25].

After failure of the conservative treatment, surgery can be an effective way of improvement for patients, especially for severe SUI. The most common surgery for SUI in women are Midurethral Sling procedures, which appear to be the most effective overall for more than 20 years now[26]. In this surgery, a small strip of material is placed under the urethra to prevent it from moving downward during activities. It acts as a hammock to support the urethra. The retropubic suspension is a supplement option if the patient cannot have sling therapy[27]. The urethra was also supported by parameters sutures suspending the vagina from the pelvic side wall. Anterior vaginal repair was taken if the pelvic floor organ prolapsed. An artificial urinary sphincter (AUS) is using an inflatable cuff placed around the urethra connected to a hand−controlled pump that allow to pass urine[28]. It is highly recommended for males with moderate−to−severe SUI by EAU[29]. AUS is considered the gold standard surgical treatment for male stress urinary incontinence and urinary incontinence that develops as a surgical complication after e.g., prostatectomy, cystectomy, and TURP[30, 31]. However, the disadvantages of these treatments, include infection or bleeding, associated to levels of complications[32]. As a less invasive surgery, bulking agents were used by injection of substances in the wall of the urethra to provide stronger support at the bladder neck, which

guarantee a short−term benefit for 1−3 years[33, 34]. Repeated injection therapy can maintain urinary continence. But the median durability and biocompatibility of the implants still fell short of expectations. Although high cure rates have been reported in SUI surgeries, a large number of females are willing to live with their condition rather than accept this invasive option. Moreover, actual standard conservative and surgical therapeutic modalities are offering a symptomatic relief without treating the underlying disorder. SUI is a condition caused by severe reduction of sphincter performance due to loss of muscle cells or muscular enervation. Complications of urinary retention, worsening urgency symptoms and erosion/extrusion of meshes have been reported. There is still a considerable number of patients that don't gain sufficient improvement by existing therapies. Therefore, to explore how to achieve better long−term treatment effects with less invasive operation, SUI cell therapy is highly anticipated to discover the possibility as a preclinical and clinical feasibility study[35-38].

Stem cells, as one fundament of regenerative medicine, are discriminated as embryonic and adult stem cells. Their basic functions include self−renewal, multi−differentiation capacity and – depending on the type of stem cell – other aspects too. Although embryonic stem cells are pluripotent so that they could differentiate into more types compared to adult stem cells, the oncogenic and immunogenic effects limit their use for therapy. In addition, ethical considerations also prohibit the use of this type of cells in human therapy. At large, two distinct types of adult stem cells have been employed in both preclinical as well as clinical studies. On one hand, mesenchymal stromal cells (MSCs) are believed to act *in situ* mainly by release of growth factors (such as TGFβ, EGF, FGF), exosomes, and in support of tissue regeneration and improving smooth muscle function. In many pre−clinical and clinical studies bone marrow MSCs (bmMSC) or adipose tissue−derived stromal cells (ADSCs) were used. ADSCs harvested by less invasive

procedure are considered as an optimal source for clinical applications. Injecting ADSCs restored urethral sphincter function and induced myogenic differentiation, nerve regeneration, and neovascularization at the implantation site[39]. On the other hand, muscle−derived cells, which also called myogenic progenitor cells, skeletal muscle−derived cells, and myoblast were applied to possibly regain the function of the striated rhabdosphincter muscle in the urethral closure complex. Muscle−derived cells (MDCs) have been investigated in several preclinical studies for SUI treatment[40-42]. These cells were able to reconstitute the contractions of the sphincter by forming myotubes[43]. MDCs also supported the recovery of functional innervation as well as growth of new blood vessels, muscle fibers[44]. The disadvantages include a long time of cell preparation for obtaining sufficient numbers cells for autologous injection and the potential risk of loss of their regenerative potential during expansion *in vitro*[45-47].

Promising preclinical studies of SUI cell therapy have been reported, but most of them used small animal models and few studies with large animals[48]. Visualizing by a cystoscope, stem cells were injected by needle with minimal invasive methods at the sphincter complex in recent animal studies. However, the evidence showed, that needle injection often leaded to misplaced cells[49, 50]. Needle injection is difficult and even an experienced operator can hardly avoid loss of cells due to full penetration of the needle through the urethral sphincter[36, 51]. Therefore, a novel technology based on a WaterJet (WJ) was developed to provide precise cell injections at the urethral sphincter. In recent studies, ADSCs were gently transported in isotonic buffers in the sphincter muscle by WJ. Growth factors or other components were used to promote cell attachment at the side of injection[52, 53]. For WaterJet injections a prototype, ERBEJET 2 (ERBE), generated an appropriate pressure to open minimal cavities smaller than 500 μm in diameter by the jet. Under the guidance of the cystoscope, even an inexperienced operator only

needs to point the jet nozzle at the target area in the urethra without any direct contact to the tissue. Then the injection can be performed simply and accurately with predetermined settings for pressure and volume of the liquid. In view of the exploration of various tissue types by the prototype, selecting appropriate injection pressure allows the injected cells to precisely reach the intended injection site, avoiding full penetration at urethral[53]. Additionally, compared to solid injection needles, the WJ does not punch a "big hole" at the target tissue. This advantage reduces any loss of active ingredients due to reflux and tissue damage, inflammation, or urine entering the submucosa[49, 50]. To explore whether the MDCs by WaterJet injection was a potential therapy for regeneration of the function of muscle tissue, we need to investigate whether myoblast could be transported with sufficient viability by WJ injection in cadaveric sample (CS) first, then in living animals (LA) as well, followed by experiments to investigate in the cells injected by WJ remained intact. In this study, we provide evidence that the novel WJ is a fast, precise and easy−to−use way to inject living MDCs in tissues with wider and diffuse distribution and less disintegration of the tissue targeted, and at higher success rates.

2 Materials and Methods

2.1 Equipment

Table 1: Equipment

Equipment	Manufacturer
Axiovert 200M Microscope	Zeiss
Axiovert A1 Microscope	Carl Zeiss
Aquarius TT system	Laborie Medical, Enschede, NL
Biological Safety Cabinets MSC 1.5	Thermo
Cell Incubator	Binder
Centrifuge 5424	Eppendorf
Centrifuge Allegra 64R	Beckman Coulter
Cryostat CM1860 UV	Leica
Electrophoresis	peQlab
ERBEJET’ 2	Erbe Elektromedizin GmbH
FVL−2400N Euro Plug	Biosan Sia
Heating and stirrer	Heidolph

In Vivo Imaging System (IVIS)	PerkinElmer
Lightcycler 480−II	Roche
LSM 510 Laser Microscope	Zeiss
Microwave	Sharp
Nano Photometer NP80	Implen
Oszillater	Heidolph
Pipes	Hirschmann
Platform Scale 440−47N 0.1 g	KERN
Platform Scale 770 1 mg	KERN
Power Pack P25	Biometra
Refrigerator −80°C	Sanyo and Skadi
Refrigerator 4°C and −20°C	Liebherr
Rotina 420R	Hettich
Staining jar	Glaswerk Wertheim
Stirrer Reax Top	Heidolph
Thermomixer comfort	Eppendorf

Theromal Cycler UNO−2	Biometra
Water Bath WBT 22	MedingLab
Transilluminator T1 1	Biometra
William’s Needle	Cook Medical
64R Centrifuge	Allegra™

2.2 Consumables

Table 2: Consumables

Consumables	**Company**
2 mL Serological Pipet	Falcon
48 well cell culture cluster	Corning
6 well culture plate	Greiner Bio−one
96 well Plate	Corning
C−Chip DHC−N01	NanoEnTek
Comber[10] test M	Roche
Cover glasses	R.Langenbrinck

Cryostat CM 1860 UV	Leica
DAKO pen	DAKO
Descosept Sensitive	Dr. Schumacher
Disposable Scalpel 20x	Feather
Disposal Bags	Brand
Filter Tips 200 µl	Biosphere Plus
Flask 250ml 75 cm^2	Falcon
Inject−F 1 ml	Braun
Lightcycler 480 Multiwell Plate 96, White	Roche
Medical Examination Gloves	Abena
Microlance 3 (0.7 * 30 mm)	Becton Dickinson
Microscope Slides	R.Langenbrinck
Microtome Blades 819	Leica
Parafilm	Pechiney
Pipette 5 ml, 10 ml, 25 ml, 50 ml	Corning
Precision Wipe	Kimtech Science

Premium Tips 1 mL (free of Dnase and Rnase)	Biozym
Safeguard 10 µl	PeQLab
Safe−lock Tubes 2.0 ml	Eppendorf
T−DOC® 7 Fr Dual Sensor Catheter	Laborie
Tubes 15 ml, 50 ml	Greiner Bio−one
X−well Tissue Culture Chambers	Sarstedt AG

2.3 Chemicals, enzymes, reagents

Table 3: Chemicals, enzymes, reagents

Material	Supplier
Anti−Desmin: rabbit IgG	Abcam, ab15200
Anti−Fast Myosin Skeletal Heavy chain Antibody: rabbit IgG	Abcam, ab91506
Anti−slow Skeletal Myosin Heavy chain Antibody: A Mouse IgG	Abcam, ab11083
(FITC) Affinpure F(ab')2 Fragment Donkey Anti−Rabbit IgG(H+C)	Jackson Immuno Research, 711−096−152
Donkey F(ab')2 Donkey Anti Mouse IgG H§L (Alexu Fluor 488)	Abcam, ab181289
FBS Fetal Bovine Serum	Sigma

Invitrogen	Thermo
Rnase Fibrous Tissue Mini Kit	Qiagen
Dnase Blood and Tissue kit	Qiagen
Lightcycler Uracil−DNA Glycosylase	Roche
Advantage RT−for−PCR kit	Takara
Lightcycler 480 SYBR Green I	Roche
Rnase−free Dnase Set	Qiagen
LE Agarose	Biozym
Tween 20	Sigma
Phalloidin−iFluor 488 Conjugate	AAT Bioquest
DMEM(1X) Dulbecco’s Modified Eagle Medium	Gibeo
Trypsin−EDTA solution	Sigma
DPBS Dulbecco’s phosphate Buffered Saline	Sigma
Percoll	Sigma
Calcein AM	Thermo
Ethidium Homodimer − 1 (EthD − 1)	Thermo

BacMam 2.0 Nucleus−GFP	Thermo
PKH 26	Sigma
PBS tablets	Medicago
Vectashield Hardset (DAPI)	Vector
Hematoxylin QS	Vector
Certistain Eosin G (yellowish)	Merck
Seed red	Morphisto
Phosphor tungstic Acid	Morphisto
Aniline blue−Orange G	Morphisto
Vectamount Permanent Mounting Medium	Vector
Tissue Freezing Medium	Leica

2.4 Buffers and solutions

Table 4: Buffers and solutions

Buffer	Ingredients
2% Gelatin solution	4 g Gelatin
	200 mL Ampuwa water

0.1% Gelatin solution	2.5 mL 2% Gelatin solution
	47.5 mL PBS
PBS−D	144 mm NaCl
	25 mm Glucose
	5.4 mm KCl
	14 mm Sucrose
	5 mm Na_2HPO_4
	5 mL Pen./Strep.
	Titrate with NaOH to pH 7.4
Transportation medium	PBS−D
	10% Pen./Strep.
	10% Fungus zone
Digestion solution for tissue degradation	HBSS 234 ml
	0.2% Collagenase mix I 4,3 mL + II 1,7 ml
	0.01% Dnase 1 30ml
	0.025% Trypsin 30 mL
10% Collagenase I	1 g Collagenase I
	100 mL HBSS
0.1% Dnase 1	100 mg Dnase 1
	100 mL HBSS

20% Percoll	7.5 mL Percoll
	30 mL PBS Biochrom
60% Percoll	6 mL Percoll
	4 mL PBS Biochrom
Growth medium	50 mL Horse serum
	50 mL 10% FCS
	5 mL glutamine
	5 mL Penicillin Streptomycin
	5 mL Fungus zone
	385 mL DMEM high glucose
Freeze medium	50% Growth medium (5 ml)
	40% FCS or plasma (4 ml)
	10% DMSO (1 ml)
Master mix (6.5 µl) for	4 µL 5x Buffer
reverse RNA to cDNA	0.5 µL Rnase inhibitor
	1 µL dNTP mix
	1 µL reverse transcriptase
Master mix (18 µl) for qRT−PCR	10 µL Sybrgreen
	6 µL NTC water
	2 µL Primer mix

Primer mix	400 µL NTC water
	50 µL Forward primer
	50 µL Reverse primer
PBS/0.1% Tween20	1 L PBS
	1 mL Tween20
5% Milk powder	0.5 g Milk powder
	10 mL PBS/0.1% Tween20
0.1% BSA/PBS	200 µL 25% BSA
	50 mL PBS
100 bp Ladder	30 µL bp−Ladder
	80 µL Loading buffer
	50 µL ddH_2O
0.1% Eosin	0.1 g Certistain Eosin G
	100 mL 99% Ethanol
Minus Medium for PKH 26	500 mL DMEM HG 4.5 g/L
	5 mL Fungi Zone
	5 mL Glutamine
	5 mL Penicillin + Streptomycin

2.5 Primer sequences

Table 5: Primer sequence

Gene	Size (bp)	Forward primer	Reverse primer	Citation
MSTN	141	CCCGTCAAGACTCCTACAACA	CACATCAATGCTCTGCCAA	Primer−BLAST
ACT	160	CGGGCAGGTCATCACCATC	CGTGTTGGCGTAGAGGTCCTT	Primer−BLAST
Myf−5	135	GCTGCTGAGGGAACAGGTGGA	CTGCTGTTCTTTCGGGACCAGAC	Primer−BLAST
Myf−6	189	CGCCATCAACTACATCGAGAGGT	ATCACGAGCCCCCTGGAAT	Primer−BLAST
MyoD1	145	CACTACAGCGGTGACTCAGACGCA	GACCGGGGTCGCTGGGCGCCTCGCT	Primer−BLAST
Desmin	176	ACACCTCAAGGATGAGATGGC	CAGGGCTTGTTTCTCGGAAG	Primer−BLAST
Myl−1	198	CTCTCAAGATCAAGCACTGCG	GCAGACACTTGGTTTGTGTGG	Primer−BLAST
B2M	261	ACGGAAAGCCAAATTACCTGAACTG	TCTGTGATGCCGGTTAGTGGTCT	Primer−BLAST
Sry	133	GACAATCATAGCTCAAACGATG	TCTCTAGAGCCACTTTTCTCC	Primer−BLAST

2.6 Fluorescence spectrum

Table 6: Fluorescence spectrum

Reagent	**Spectrum** (nm)		**Settings on laser** (nm)	
	Excitation	Emission	Excitation	Emission
DAPI	360	460	405	BP 420−480
Bacmam	488	520	488	BP 505−550
Phalloidin−iFluor 488	491	516	488	BP 505−550
Calcein Am	494	517	488	BP 505−550
Ethidium homodimer−1	528	617	543	LP 615

PKH 26	551	567	543	LP 560
Transgene	*	720	488	LP 560

2.7 Software

Table 7: Software

Software	Distributor
Endnote X9	Thomson Reuters
Microsoft Office (Word, Excel, PowerPoint)	Microsoft
ImageJ	National Institutes of Health
Prism 8	GraphPad Software
Image Composite Editor (ICE)	Microsoft
LCOT 1.5.0 SP4	Roche
AxioVision Rel. 4.8	Zeiss
Multiple Task Urodynamics System Version 11	Laborie Medical Technologies
Zeiss 2009, 2011(black, blue edition), 2.6	Zeiss

2.8 Isolation of porcine muscle−derived cells

2.8.1 Prepare gelatin−coating plate

For expansion of porcine muscle−derive cells (pMDCs), cell culture vessels had to be coated by gelatin[54]. To this end, 2.5 mL 2% gelatin solution were pre−heated at 37 °C for 0.5 h and then diluted to a 0.1% solution with 47.5 mL PBS. For coating of a 6 well plate 2 mL/well, for coating of flasks, 10 mL/T75 flask of 0.1% gelatin solution were added and incubated at 37°C for 30 min. The coating solution was aspirated, and the vessels were air dried for 2−3 h with the lid open under the sterile bench. Coated vessels were stored at −20°C.

2.8.2 The sacrifice of male piglets for isolation of muscle tissue

4−5 days old male piglets were sedated by a veterinarian by i.m. injection of Atropine and Azaperone. After initial sedation, Midazolam and Ketamine were applied i.m. to establish deep anesthesia. In deep anesthesia the animal was sacrificed by injection of KCl i.v.. The skin was sterilized and access to the *M. semitendinosu*s and to subcutaneous fat was prepared by aid of forceps, scalpel, and scissors. Tissues were harvested aseptically and transported in 50 mL tubes with transport medium on wet ice. The animal study was approved by the State of Baden−Württemberg Animal Welfare Authorities under file number CU1−16, and the Bavarian State Authorities under file number ROB-55.2-2532.

2.8.3 Isolation of porcine muscle−derived cells

Established protocols were followed to prepare porcine MDCs (pMDCs)[55]. In brief, in the lab's vertical class II clean benches, the muscle was rinsed in fresh medium for 2 min. (approx. 5 g wet weight per batch). Then the muscle was place in a Petri dish, covered with medium to wet the cells, and cut with scissors and

scalpel into small pieces. The material was collected with PBS, split in 2 fractions for proteolytic digestions, and sedimented by centrifugation (800 g, 15 min, 4°C). The supernatant was removed and 25 mL of digestion solution per tube were added. The tissue was digested on the shaker (37°C, 20 min., 800 rpm) Then, the tubes were cooled on ice for 2 min., 20 mL of MEMα medium were, mixed and the suspension was filtered through 100 µm cell filter. Undigested material was further process by two additional rounds of proteolysis and filtered again. The resulting filtrate was centrifuged at 800 g, 4°C for 10 min. to collect the pMDCs. The cell pellet was resuspended in 5 mL MEMα and then placed on ice. Each tube was rinsed MEMα again and the resulting cell suspension was filtered through a 70 µm cell filter and cells were centrifuged at 800g, 4°C for 10 min. The pellet was then resuspended in 12 mL PBS. 1.5 ml 60% Percoll solution were added in 15 mL centrifugation tube first. Then 11.5 mL 20% Percoll solution were layered very slowly above. At last, 2 mL cell suspension was layered on top. After centrifugation (RCF: 11000 g, 15 min., 4°C, Rotor C1015, Allegra™ 64R Centrifuge; low acceleration without brake), the greasy top layer was aspirated, and cells were collected at the interface between the 20% and 60% Percoll solution with a Pasteur pipette (about 2 mL per tube). The cells were diluted with 14 mL MEMα, centrifuged at 700g 4°C for 10 min., and the supernatant was discarded. 10 mL MEMα were filled into the tube to resuspend and wash the cells again. The pellets were resuspended with 15 mL growth medium seeded in in gelatin−coated wells.

2.9 Expansion of porcine muscle−derived cells

2.9.1 Passage of porcine muscle−derived cells

Gelatin−coated cell culture vessels were prepared one day before use (see 1.8.1.). To passage cells, the medium was aspirated with a Pasteur pipette and adherent

cells were washed twice with PBS[56, 57]. By this, not adherent cells and debris were removed. For detachment of pMDCs, 3 mL Trypsin/EDTA were added and the flask was placed in the 37 °C incubator for 3 min. Detachment of the cells was confirmed by microscopy, 3 mL culture medium (*Table 4*) were added to stop the proteolysis, and the cell suspension was transferred into a 50 mL centrifugation tube. The cells were sedimented (1500 rpm, RT, 7 min.), the supernatant was discarded, cell pellets were resuspended in 10 mL culture medium and counted in a Neubauer counting chamber (C−Chip DHC−N01)(*Table 2*). After mixing 20 µL trypan blue and 20 µL cell suspension in a 96 well plate, trypan blue – cell mixture was filled into the counting chamber properly. The four outer corner squares were counted with “white” = alive cells vs. “blue” = dead cells according to the "L principle" using the formula: $The\ viable\ cell\ concentration = n \div 2 \times 10^4\ cells/mL$. The cells were seeded as the concentration of $2 \times 10^5\ cells/mL$ in the gelatin coated vessels or $500\ cells/ml$ in chamber slides and cultivated until reaching 70%−80% of confluency.

2.9.2 Medium change of porcine muscle−derived cells

For medium changes, the medium was aspirated with a Pasteur pipette (*Table 2*) and 10 mL of growth medium (*Table 4*) were added to the cells. The medium was changed routinely twice a week.

2.9.3 Freeze cells

Cells were detached by trypsin as mentioned in 3.1 and centrifuged. The supernatant was removed, and the pellets were resuspended with 1.5 mL ice−cold freezing medium. The cells were transferred in cryopreservation tubes, slowly cooled to −20°C, and then stored for no more than 4 weeks at −70°C until further use. For long−term storage, the cells were transferred to a liquid nitrogen tank.

2.9.4 Defreeze cells

Cell cryopreservation tubes were transported on wet ice to the lab, moved by hand in the 37 ℃ water path (*Table 1*) for 1 min. Then cell suspension was poured into a prepared 10 mL centrifuge tube containing 4 mL culture medium. After centrifuging at 1500 rpm for 7 min, cells were resuspended in 10 mL culture medium. Finally, cells were counted and seed into bottle or chamber slide appropriately

2.10 Characterization of porcine muscle−derived cells

2.10.1 Detection of the pSRY gene in cryosection samples by PCR

2.10.1.1 DNA extraction from cryosections

To corroborate the injection of male cells in the female animal, cryosections of the region of interest were prepared. Tissue was scraped off by a scalpel from 4 consecutive cryosections and placed in the 1.5 mL centrifugation tube. To isolate DNA a kit was used (Qiagen, DNeasy, Blood & Tissue kit, REF: 69504). 180 µl ATL buffer and 20 µl proteinase K were added and incubated under agitation at 56°C for 1 ~ 3 h (or overnight) on the thermomixer. 200 µl AL buffer were added and mixed (Vortex) for 15 s. Then 200 µl 100% ethanol was added by pipette and mixed. The entire 600 µl liquid were pipetted into a DNeasy Mini Spin Column (No. 1011707) and centrifuged at 10000 rpm for 1 min. The flow−through fraction was discarded, the column was put on a new tube. 500 µl AW1 buffer were pipetted into the column and then centrifuged at 10000 rpm for 1 min. The column was moved in a new tube again. 500 µl AW2 buffer was pipetted into the column and then centrifuged at 20000 rpm for 3 min. The column was moved in a new 1.5 mL centrifugation tube included in the kit. For extraction of DNA, 100 µl AE buffer

were pipetted directly on the membrane and incubated at room temperature (RT) for 1 min. Finally, centrifugation at 10000 rpm for 1 min, DNA was measured by UV spectrophotometry at 260 nm (Nanodrop) and the DNA solution was stored at −20°C.

2.10.1.2 Polymerase chain reaction to detect the SRY gene

Prior to pipetting a PCR reaction, the workplace was cleaned by DNA−ExitusPlus™ IF (A7409, 0500, Applichem GmbH). All reagents including Sybr green, non−template water, DNA and premier mix (*Table 5*) were mixed well, centrifuged, and cooled on ice before use. 2 µL of the scraped off DNA solution were pipetted in a well of a specific 96−well plate. For controls, 2 µL non−template water, or 2 µL of "positive male control" DNA solution, or 2 µL "negative female control" DNA solution were added to separate wells. Then 18 µL master mix (*Table 4*) were added to the respective wells. After sealing the 96−well plate tightly to prevent the liquid evaporating in the PCR machine, it was centrifuged at 1000 rpm for 1 min and kept at 4°C to set the program of the Lightcycler480−II PCR machine as described in *Table 8* .

Table 8: Features of pSRY qRT−PCR

Effect/Reaction	Temperature	Time	Cycles
Denaturation	95°C	10 s	1
Amplification	94°C−58°C−72°C	30 s–30 s–20 s	50
Primer Extension	72°C	5 s	1
Melting Curve	95°C−60°C−97°C	5 s–30 s–cont.	1
Cooling	40°C	30 s	1

2.10.1.3 Analysis of PCR products by gel electrophoresis

To prepare a 2% agarose gel for DNA electrophoresis[58], 1 g agarose was added into a conical flask with 50 mL 1x TBE buffer. After covering with cling film, the conical flask was boiled in the microwave oven for approx. 5 min until all agarose was melted and no more streaks were seen. 5 µL Gel Red Nucleic Acid stain was added. The agarose was mixed by magnetic stirrer and cooled to approximately 60°C. The gel was poured into the mold and left for 20 min to harden. 10 µL pSRY gene PCR product were mixed with 4 µL loading buffer and 10 µL mix was added in gel's pocket. 10 µL 100bp ladder were used as DNA size reference. Then the gel electrophoresis was run for approximately 40 min at 100 V/0.1 A and stopped before the blue band run out of the gel. The DNA bands were visualized by UV light and recorded by a cell phone camera. A PCR product of 133bp of length in male DNA is proof of the pSRY gene.

2.10.2 Quantitative Real−time polymerase chain reaction (qRT−PCR) for transcript analyses

2.10.2.1 RNA extraction

For isolation of RNA from cells, cells were washed, detached, and pelleted as described in section 1.9.1. Then, cells were resuspended, washed with 10 mL cold PBS and sedimented again. The supernatant was removed. Remaining liquid was aspirated carefully and the cell pellet was resuspended in 350 µL RLT buffer complemented by ß−mercaptoethanol to isolate RNA as described by the manufacturer (Qiagen, RNeasy kit). The extract was stored for 2 hours at −70°C, homogenized by aspiration with a syringe and G20 needle, mixed with 350µl 70% ethanol, transferred to the RNA−extraction column (Qiagen, RNeasy kit), and centrifuged at 10000 rpm for 15 sec at RT. The flow−through was discarded, 350

µL RW1 (washing buffer) were added to the column and centrifuged at 10000 rpm for 15 sec at RT. The flow−through was discarded again and 80 µL of DNase were added to the column and incubated for 15 min at RT. 350 µL RW1 buffer were added to wash out the DNase by centrifugation at 10000 rpm for 15 sec. The column was placed on a new 1.5 mL centrifugation tube before adding 500 µL RPE buffer. The sample was centrifuged at 10000 rpm for 15 sec., the flow−through was discarded and 500 µL RPE buffer were added and centrifuge 2 times to remove any debris. Finally, the column was placed in a new1.5 mL centrifugation tube, loaded with 40 µL RNase−free water, incubated for 1 min and centrifuged at 10000 rpm for 1 min. The flow containing RNA was stored at −70°C until determination of the yield and prior to reverse transcription into cDNA.

2.10.2.2 Reverse transcription of RNA into cDNA

RNA extracts were retrieved from −70°C and put on ice. 1 µL RNA from each sample was used to measure the RNA concentration (C_{RNA}) by absorption of ultraviolet light at a wavelength of 260 nm in spectrophotometer (Nanodrop). The RNA volume (V_{RNA}) was calculated by Excel following the formula $V_{RNA} = \frac{1000\ ng}{c_{RNA}\ ng/\mu l}$. According to the V_{RNA}, up to 12.5 µL of the RNA extract were mixed with the corresponding volume of DEPC water (Rnase−Free Dnase Set, QIAGEN) to yield 12.5 µL of RNA solution for cDNA synthesis. The samples were mixed and centrifuged. Then 1 µL oligo dT primer (*Table 5*) solution were added, mixed well, sedimented by centrifugation, and put on ice. In a PCR block, the samples were heated at 65°C for 2 min to unfold the RNA molecules, and quenched on wet ice. Then, 6.5 µL of the master mix were added (*Table 9*), mixed, centrifuged again and placed on ice. The PCR block was warmed up to 42°C, the samples were put in the device and incubated at 42°C for 1 h for cDNA synthesis, and cooled to 4°C

in the device. Finally, 80 µL DEPC water were added, mixed, and the cDNA was stored at −20°C.

Table 9 Master−mix for reverse transcription of RNA to cDNA

Reagent	Volume
5x Buffer	4 µl
RNase inhibitor	0.5 µl
dNTP mix	1 µl
Reverse transcriptase	1 µl

2.10.2.3 Quantitative Real−time polymerase chain reaction (qRT−PCR) of cDNA

The worktable was cleaned by DNA−ExitusPlusTM IF (A7409, 0500, Applichem GmbH) before a PCR reaction. All reagents including Sybr green, non−template water, cDNA and primer mix mixed well, centrifuged, and cooled on ice before use. 2 µL cDNA was first pipetted in a well of Lightcycler 480 Multiwell Plate 96, White. For controls, 2 µL non−template water for each negative control, or 2 µL SMC cDNA as positive control for machine identification, were added to separate wells. Then 18 µL master mix (*Table 4*) were added to the respective wells. After sealing the 96−well plate tightly to prevent the liquid evaporating in the PCR machine, it was centrifuged at 1000 rpm for 1 min and kept at 4℃ to set the program of the Lightcycler480−II PCR machine as described in *Table 10*.

Table 10 Features of characterization marker gene by qRT−PCR

Program	Temperature	Time	Cycles
Denaturation	95°C	5 s	1
Amplification	95°C−60°C−72°C	10 s–20 s–30 s	39
Melting Curve	95°C−60°C−97°C	5 s–30 s–cont.	1
Cooling	40°C	30 s	1

2.10.3 Immunofluorescence of cells

After cell harvesting, cell were counted and resuspended at 4×10^4 cells/mL in cell culture medium (see section 1.9.1). Then 500 µL cell suspension, corresponding to 2×10^4 cells, were added in each well of the gelatin−coated chamber slides and cultured up to 70% ~ 80% of confluence. For fixation, medium was aspirated, cells were washed twice with cold PBS, and 200 µL/well of ice−cold methanol were added[59]. The samples were incubated at −20 °C for 10 min. Then, the methanol was removed and the samples were air dried at RT for 10 min. and stored at −20 °C. For staining of the cells with antibodies, the samples were wash 3 × 4 min. at RT with 500 µl PBS/0.1% Tween20, then, 500 µL 5% milk powder in Tween/PBS were used to block unspecific antibody binding at RT for 30 min. The samples were then washed 3 times with PBS/0.1% Tween20. The antigen detecting antibody, i.e., so−called first antibody, was diluted with 0.1% BSA/PBS to the desired concentration. For detection of Desmin (1 : 200), Fast myosin (1 : 200), or Slow myosin (1 : 100) different dilution were employed (*Table 3*). 100 µl of the diluted first antibody was added in each well and incubated at RT for 90 min in a humidified chamber. For “negative controls” 100 µl 0.1% BSA/PBS instead of an

antibody were added to a separate well. After incubation, samples were washed 3 times with PBS/0.1% Tween20, and 100 µl of detection antibody, i.e., so−called second antibody FITC−labeled anti−rabbit 1: 100; Alexu Fluor 488−labeled anti−mouse 1: 2000 in 0.1% BSA/PBS were added and incubated at RT for 45 min in the humidified chamber. The slides were washed again before the chambers were detached and dried at RT for 20 min. Finally, slides were mounted with hard−set (Vectashield), and images were obtained by confocal laser scanning microscopy (Zeiss LSM 510) (*Table 6*).

2.10.4 Labeling of porcine muscle−derived cells

2.10.4.1 Live/dead stain (Calcein AM and EthD−1)

Prior to staining of cells with a Live/Dead Viability/Cytotoxicity Kit (Thermo Fisher, L3224)(*Table 3*), adherent pMDCs were washed 3 times with PBS and the supernatant was aspirated carefully. For staining of the cells, 20 µL of the supplied 2 mM EthD−1 stock solution (component B) was mixed with 10 mL of D−PBS and added to the cells. Then 5 µL of the 4 mM Calcein AM stock solution supplied (component A) were added, mixed, and incubated at RT for 30 min. Then, cells were harvested as described above (1.9.1) and stored in an ice box for further use.

2.10.4.2 Labeling of pMDCs by a baculoviral expression system (BacMam2.0)

Cells were harvested, washed, and seeded in expansion medium at the desired cell density to grant optimal transformation by the virus as described by the manufacturer (CellLight^{TM} Talin−GFP, BacMam 2.0, Thermo Fisher, C10611). Cells were incubated for approx. 3 h for attaching. Then, 2 µL BacMam reagent was added for per 10^4 cells in medium and incubated for 16 h at 37°C. To determine efficacy of staining and the percentage of fluorescent cells, the medium was replaced and the cells were observed by fluorescence microscopy with the setting

from *Table 6*. After staining, cells were washed thoroughly 3 times with medium and 2 times with PBS to remove all remaining viral particles from the media. Then cells were harvested by trypsin−EDTA, washed again, counted, diluted in injection medium and used for injections at the densities desired. This type of staining was not performed by myself but by qualified and performed at the lab.

2.10.4.3 Staining of porcine MDCs by PKH 26 dye

The pMDCs were washed 2 times by PBS at the desired cell density 5 mL of minus medium were added (*Table 4*). Then 1.8 mL per T75 cell culture flask of PKH 26 solution diluted 1:15 with PBS − which was kept in the dark and wrapped aluminum foil around the tube – were added as described by the manufacturer (PKH 26 Linker−Kit, Sigma). The reaction was incubated for 1 h at 37°C, 5% CO2, in an incubator in the dark. Then , 5 mL stop medium (minus medium complemented with 20% FCS) were added and incubated for 2min in dark. The cells were washed 2 times with 5 mL minus medium. Then, 10 mL of growth medium were added. After 3 h of incubation, efficacy of staining and the percentage of PKH 26 positive cells were detected by microscopy and recorded.

2.11 Cell injection in cadaveric urethral tissue samples

2.11.1 Preparing cadaveric samples

Fresh female porcine cadaveric organs of the urinary tract including kidney, ureter, bladder, and urethra were obtained from the abattoir by courtesy of Erbe Ltd. Excess tissue was removed, bladder and urethra were prepared, and cooled in bags in PBS on wet ice until use. Placing the trigonumvesicae face up, an urethral catheter was inserted into the urethra for fixation of the anatomical position and protecting the lower part of urethra. Then the urethra was cut along the dorsal midline by scissors.

2.11.2 Injection cells by WJ E_{60-10} or WN into cadaveric urethra

6×10^5 Calcein AM/EthD−1 stained cells or male pMDCs from iRFP−transgenic pigs were injected at a suitable location into the urethra 5 ~ 10 cm from the internal urethral orifice by William's Needle (WN) in acute angle or by WaterJet E_{60-10} perpendicularly as recently described[52]. A drop of glue was placed on the injection port to prevent cell suspension flow back through the injection hole. Half of the samples from each group were used to retrieve cells from the tissue by syringe aspiration and continued culture of the cells. The other tissue samples were trimmed to reduce their size and placed vertically in the freezing mold, with the distal tissue at the bottom (*Table 11*). The samples were covered with Tissue Tec freezing media immediately and either frozen in liquid nitrogen or in a freezer at −80 °C for further use.

Table 11: Overview on cell injections in cadaveric samples by WaterJet E_{60-10} or William's Needle

Cell source	WaterJet E_{60-10}		William's Needle	
	Extraction	Cryosection	Extraction	Cryosection
Transgene pMDCs	4	4	2	3
L/D staining Wild Type pMDCs	4	4	2	2

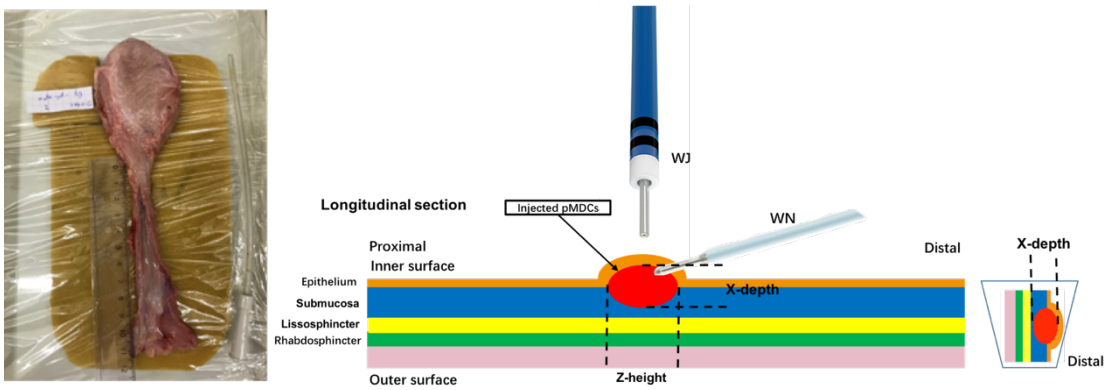

Figure 1: Injection of cells by WaterJet and William's Needle into the cadaveric urethra.
Cell suspension was delivered to the muscle layer through William's Needle or WaterJet device without full penetration. According to the direction of injection and strict sampling and embedding techniques, the injection cell mass can be accurately and uniformly measured in three dimensions, namely X−depth, Y−width and Z−height.

2.11.3 Extraction of Calcein AM− & EthD−1−stained wild type (WT) pMDCs after injection by WaterJet or William's needle in cadaveric urethra

After WJ or WN injection in cadaveric urethrae, the Live/Dead labeled pMDCs were retrieved by a syringe from half of the samples, following the path from injection. The reextracted cells were then inoculated in petri dishes within half an hour and cultured for up to five days to demonstrate their immediate viability and the ability to survive and proliferate over several days. During culture, these cells from WJ and WN injections respectively, were observed daily and photographed with transmission light channel and GFP channel by Axiovert A1 microscope (*Table 1*). Uninjected but labelled cells served as a control group. The photos were finally merged by ImageJ (*Table 7*).

2.12 Cell injections in living animals

2.12.1 Animal husbandry

Animals were kept under ethical husbandry and veterinarian supervision in the facilities of the University of Tuebingen hospital. The trial approval number is CU1/16. After surgical treatment, animals were observed on a regular basis by the principal investigator Prof. Aicher and by a veterinarian.

2.12.2 Urine test

After the animal was anesthetized and immobilized on the operating table, a cystoscope was inserted from the external urethral opening to the bladder. A moderate amount of midstream urine was collected through the excretory opening in a sterilized measuring cup for urine testing (Figure 2 A). The test strip from Combur[10] test M (*Table 2*) was totally dipped in urine briefly. Excess urine was removed. After 60 s, the test field was held vertically down to compare with the color comparison scale on the test strip tube (Figure 2 B).

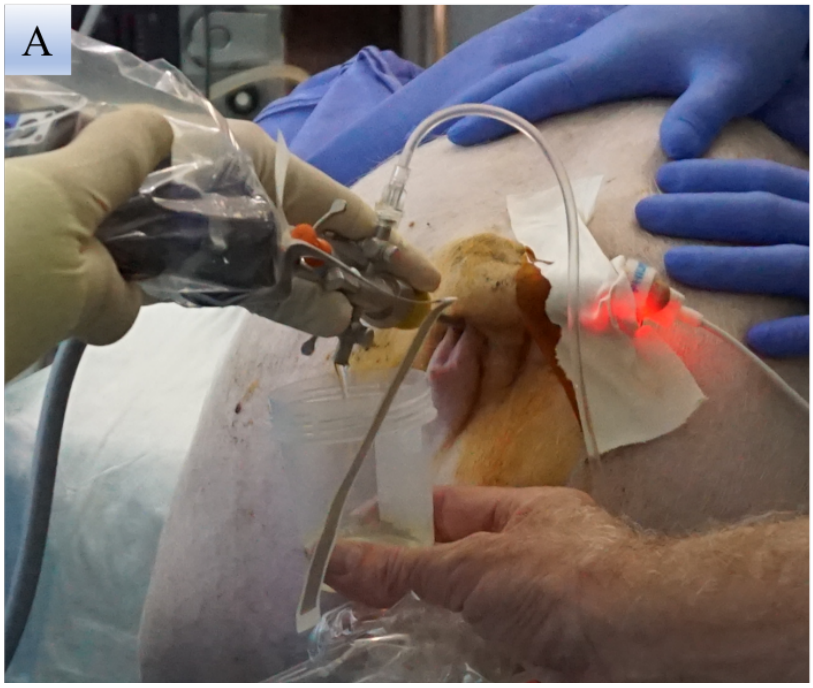

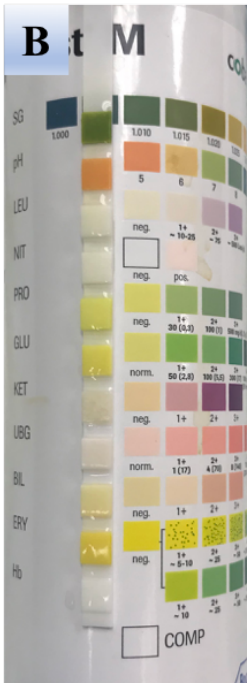

Figure 2: Urine test by Combur10 test M
(A) Urine was collected by a sterilized cup. (B) Placement direction and comparison of analysis Urine Test M.

2.12.3 Urodynamic test

Urethral wall pressure profiles (UPP) and the position of the wall pressure maximum in the urethra were measured in each individual pig before the cells were injected to facilitate an optimal injection position[60]. Urodynamics were recorded in animals placed in prone posture after anesthesia (Figure 3A). Static urethral pressure profilometry was investigated by Aquarius TT system (*Table 1*) with urodynamic catheter (Laborie Medical, Enschede, NL)(*Table 2*). After the bladder was emptied, the measuring sensor was introduced in the bladder and the urethra were perfused with 50 mL isosmotic saline. The pressure sensor was slowly retracted at 1 mm/s and the data is recorded simultaneously (Figure 3B). Proprietary software (*Table 7*) was used to collect and analyze the experimental data. Maximum urethral closure pressure (MUCP) and distances to urethra and bladder interface were calculated (Figure 3C). The position "UPP starten 1" showed catheter at the beginning of urethral, internal urethral orifice in the UPP diagrams. The position "UPP stop 1" showed catheter at the end of urethral, external urethral opening. The UPP Peak 1 was the location of MUCP.

$$Pclo = Pure - Pves$$

$$Urethral\ length = UPP\ stop\ 1 - UPP\ Startten\ 1$$

$$Continence\ zone = UPP\ Peak\ 1 - UPP\ Startten\ 1$$

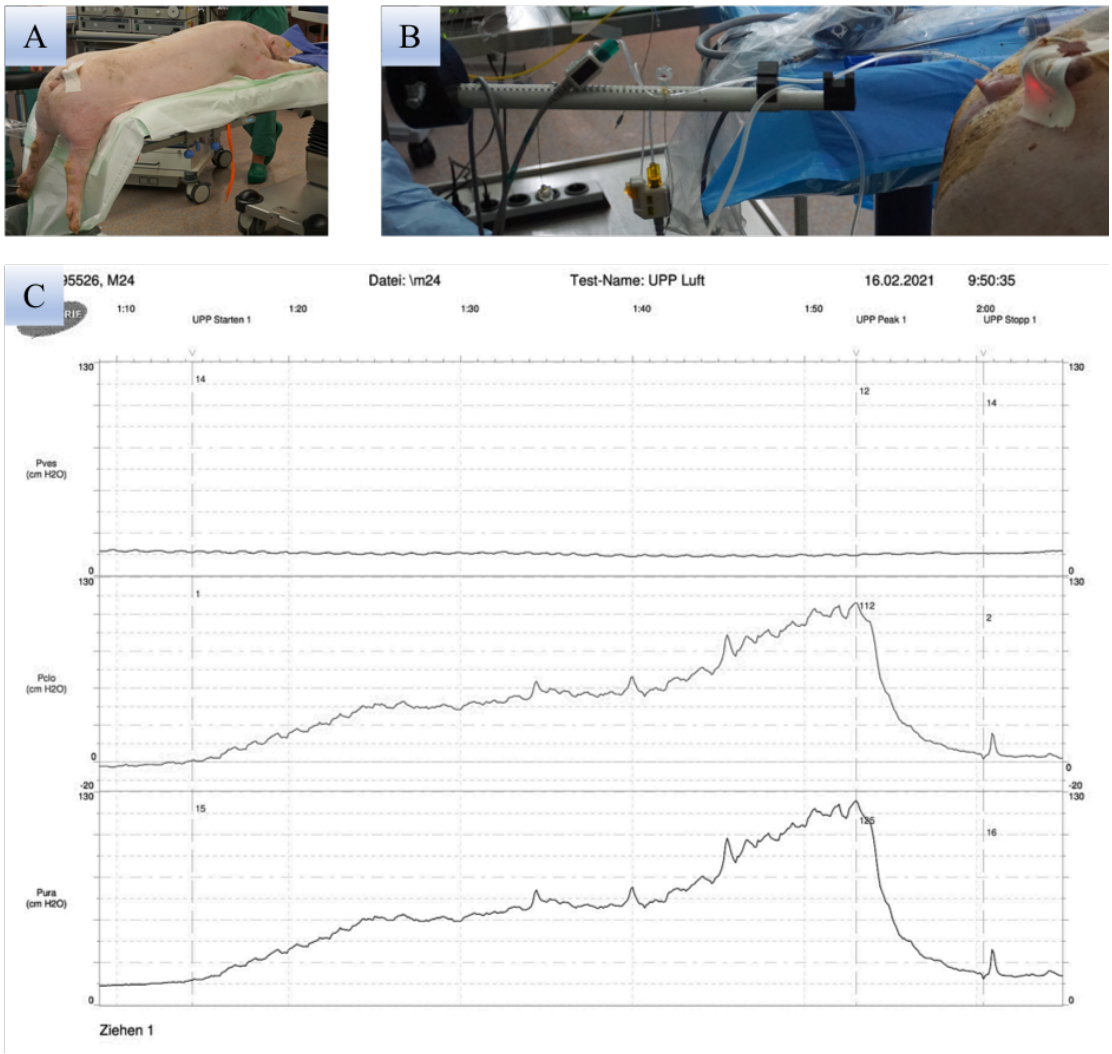

Figure 3: Method of analysis UPP

(A) The prone posture for urodynamic test. (B) Urodynamic test on pig. (C) The definition of all parameters and the position of MUCP.

2.12.4 Injection cells by WaterJet in living animals

Based on the results of the urodynamic test and with the help of the endoscope's scale, a WaterJet injection device was placed by aid of a cystoscope and under visual control through the urethra (Figure 4 A) to the position of MUCP and the cells were injected once at 3 and once at 9 o 'clock position, respectively by an angular bend of the injection nozzle (Figure 4 B). Each injection of 500 µL cell suspension contained 6×10^5 cells[49]. In this study, 18 landrace pigs were injected a pressure profile of E_{60-10} and another 6 animals with a pressure profile of E_{80-10} to yield cells

in different injection depths in the urethra[52, 53] (Figure 4 C). All living animal WaterJet injections were operated under the supervision of the PI, Prof. Aicher, by experienced urologist, Dr. med. Niklas Harland, employing a WaterJet prototype system, generously provided by Erbe Medizintechnik GmbH. After cell injections, the follow−up in this study was a few hours (sacrifice on the same day) up to 7 days post−surgery. After follow−up, animals were sedated and sacrificed in deep anesthesia by injection of KCl i.v. by a veterinarian. Immediately after sacrifice, bladder and urethra were harvested, placed in wet bags and transported on wet ice for the next experiments. Surgery on fresh porcine cadavers to prepare bladders and urethras were performed by myself under supervision of the PI Prof. Aicher.

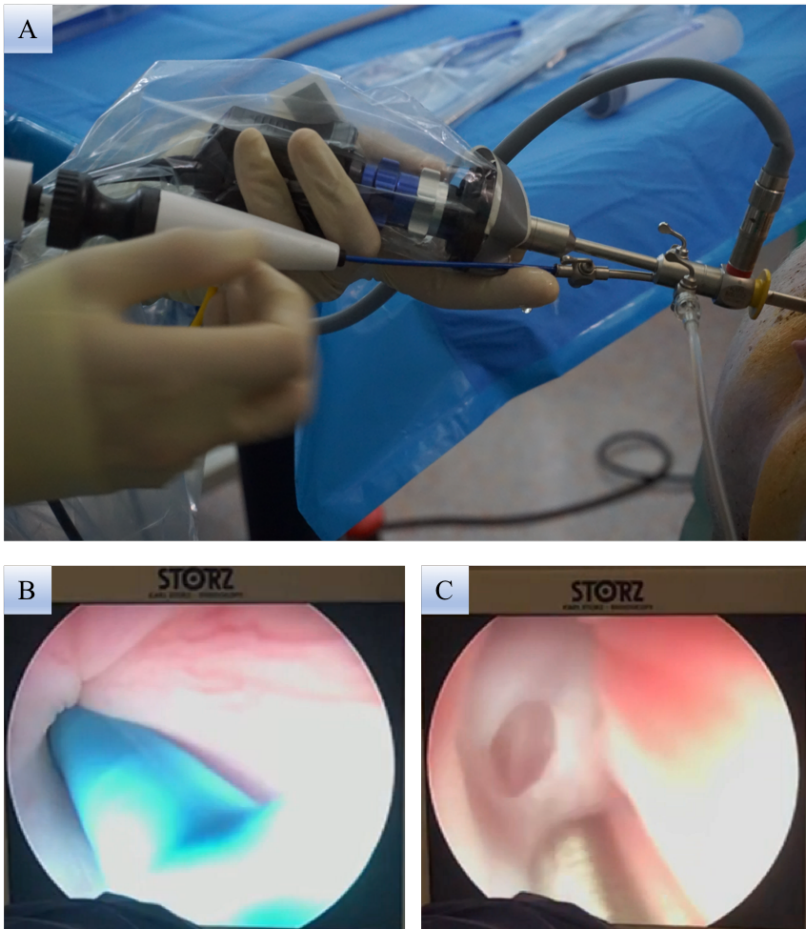

Figure 4: Operation of WaterJet injection in living animals
(A) WaterJet insertion into the urethra (B) Intra−urethral aspect of a cysoscopic WaterJet injection at MUCP. (C) The mark of a bloodless injection.

2.13 In vivo imaging system (IVIS)

In all bladder and urethra explants from WaterJet and WN injection, the position of cell injections was determined by an In Vivo Imaging System (IVIS) Spectrum; PerkinElmer, Inc., Waltham, MA, USA). The filters used were $\lambda_{ex} = 535\,nm$ and $\lambda_{em} = 580\,nm$, f2, a binning of 8. A smoothing of 3×3 pixels was displayed with appropriate fluorescent background setting[53]. According to the fluorescence signal, the part containing injected cells was separated from the urethra and quickly put into a Dewar thermocontainer filed with liquid nitrogen to generate frozen samples, transported on dry ice, and then stored in a −80°C deep freezer. The IVIS measurements were performed at the Department of Radiology, University Tuebingen Hospital under supervision and after training by Dr. Beziere. The preparation of cryosections from frozen samples from pig urethrae was performed in part by Mrs. Tanja Abruzzese.

2.14 Histochemistry

2.14.1 Hematoxylin−eosin (HE) staining

For histochemical analyses, 20 µm cryosections were generated (see below 1.15.1.). The tissue on the glass slides is surrounded by a silicon pen (REF: S2002, DAKO) to avoid spreading of reagents to the side. Hematoxylin (H−3404, VECTOR) was dropped on tissue samples and incubated for 2min. These slides were soaked in the staining jar under running tap water for 10 min and dipped in distilled aqua for 5 s. Then, 0.1% Eosin solution (C.I.45380, MERCK KGaA) were used to staining for 2 min. Then, the tissue samples were again in tap water and aqua. Samples were air−dried and slides were covered by Vectamount (Vector).

2.14.2 Azan staining

The dry cryosections were warmed up to 40°C for 15 min on a heater and then stained with Seed red solution for 25 min in the staining jar (Glaswerk Wertheim) and washed for 1 min. in distilled aqua. These slides were then stained with 5% phosphor tungstic acid solution (REF: 10324.00250, Morphisto) for 5 min and washed by aqua again. Aniline blue – Orange G (REF: 10144.00250, Morphisto) was the last staining reagent and incubated for 30 s, then washed by aqua again. Slides were air dried and covered by Vectamount. All HE & Azan stained slides were photographed with an Axiovert A1 Microscope (*Table 1*), and the Panorama pictures were manually captured and synthesized with Image Composite Editor (Microsoft) (*Table 7*).

2.15 Fluorescence

2.15.1 Frozen tissue Sectioning

The temperature of the cryostat was adjusted to −21°C to −24°C (Leica, CM1860 UV). The frozen tissue block was maintained at −24°C throughout the entire sectioning procedure. The surface of a metal tissue disc was covered with tissue freezing medium and the top of frozen sample was pressed onto it. The wet mount was placed inside the cryostat for 10 min. and the discs were fixed in the holder of the cryostat. With the setting of 20 µm cut thickness and appropriate position of the anti−roll device and razor blade, the tissue sections were generated by rotating the roller continuously at a constant speed at an ideal temperature. Pressing the tissue slides against the cryostat with a glass slide at room temperature allows the tissue graft to be transferred to the slide, as the temperature difference between the slide and the cryostat will not cause the tissue slides to stick to the cryostat. A brush was

used to clean up the remains possibly present on the frozen tissue block or the razor blade of the apparatus. The slides were stored at –80 ℃.

2.15.2 Detection of cell injected areas in cryosections by fluorescence microscope

The slides from 2.15.1 covered by DAPI with hardset (Vectashield) were observed by an Axiovert 200M fluorescence microscope to figure out the first, maximum and last layer of cells injected in the urethra (*Table 1*). After obtaining 20µm serial consecutive sections from whole tissue samples, slides at intervals of 50 sections were observed under the fluorescence microscope to verify the injected pMDCs. After observing the possible range of injected cells, the slides at 10 intervals were used to find the first, maximum, and last layers of injected cells in the cryosections more accurately. At the end, the number of layers of injected cells were pinpointed. All of the layers in the region of interest were captured by fluorescence microscope and recorded for future measurements for analysis of localization and distribution. All the setting of fluorescence spectrum as mentioned in *Table 6*.

2.15.3 Phalloidin staining to detect muscular tissue by confocal laser scanning microscopy

After successful mapping the positions of cell appearance, maximal cell density and distribution and last appearance in consecutive cryosections by fluorescence microscopy, cryosections in the range of maximal cell amounts were taken out for further analyses and warmed up at 40 ℃. To label muscle tissue, 250 µL phalloidin conjugate working solution, prepared by diluting the 1000x phalloidin conjugate in DMSO solution with PBS/1% BSA at ratio of 1 : 1000, were added to the sample and incubated in a wet chamber at RT for 90 min. Slides were rinsed with PBS 3

times, sealed, and investigated by a laser scanning microscope (Observer C1 with LSM−510 beta, Zeiss). The settings of fluorescence spectrum are showed in *Table 6*.

2.16 3 dimensional quantitively measurement of cell positions in the urethra (XYZ−3D and DISIC method)

As shown in picture 7.1, the size of injection spots (X, Y, Z dimensions) and the distance between sphincter muscle and injected cells (DISIC) in the urethra was determined in 3 dimensions. The Z−height of the cells spot by calculating the first and last layer:

$$\text{Z-height} = (\text{Last} - \text{First}) \times 20\ \mu\text{m}$$

On maximum layer, X−depth (Blue) which is the distance perpendicular to the epithelium and Y−width (Yellow) which is parallel to the epithelium was measured by the software of the microscope Zen 2.6 (Figure 5 A, D) When the injection cells were divided into multiple areas (typically seen in the WaterJet injection group), the distance were measured only including the clusters of cells without including radially scattered cells. In WaterJet injections in cadaveric samples, the injection was perpendicular to the urethra. This was different from needle injection in the cadaveric group and in comparison to the *in vivo* WaterJet injections (Figure 1). Therefore, Z−height and X−depth results in this group were changed to obtain three−dimensional directional data with the same meaning for unified statistics. For comparing WaterJet injections using the E_{60-10} and E_{80-10} protocols in the living animal study, the distance between sphincter muscle and injected cells was detected (Red)(Figure 5 A,B,C). Then the cell cluster center was automatically calculated and located by the microscopy's propriety software (ZEN, Zeiss; *Table 7*), when the boundary range of the cell cluster was manually selected.

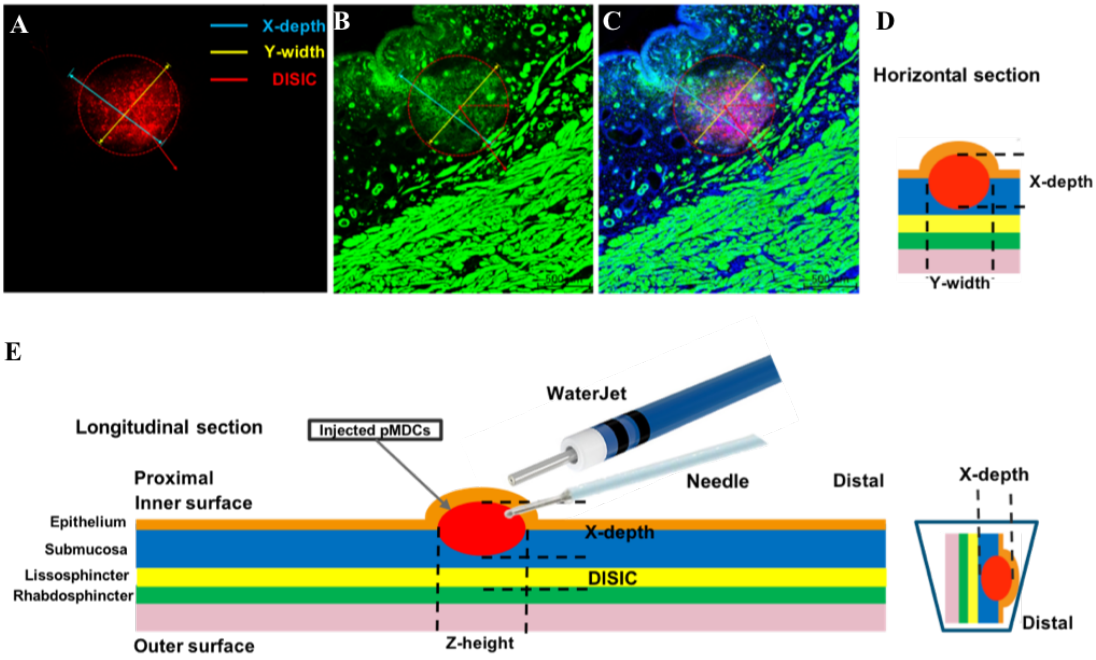

Figure 5: Method of measuring the length on three dimensions

The distance was measured only included the clusters of cells without radially scattered cells.

2.17 Statistical analysis

All statistical analyses were performed on Graph Pad Prism 8.0. Urethral pressure profilometries were analyzed using two−tailed t−tests as well as XYZ−3D & DISIC. It should be emphasized that in the distribution analysis, because of multiple factors involved, including WJ vs WN, CS vs LA, WJ E_{60-10} vs WJ E_{80-10}, a t−test was used for these three groups. A *P*−value less than 0.05 was considered statistically significant and marked in the artwork accordingly $*P < 0.05$, $**P < 0.01$, $***P < 0.001$, $****P < 0.0001$.

3 Result

3.1 Proliferation of pMDCs

Following the protocols described in detail above, the pMDCs isolated from young male pigs were seeded in the gelatin−coated flasks in primary culture, considered as passage 0 cells. When reaching a cell density of up to 70%−80% after about 10−14 days of culture, the cells were passaged to yield passage 1. Then during 5−7 days of continued culturing, the pMDCs were passaged up to passage 6. The morphological changes of growth were observed at passage 1, 2, 3 (Figure 6). The pMDCs with round nucleus and even cytoplasm were spindle−shaped at passage 1 (Figure 6A), myoblast−like at passage 2 (Figure 6B), while part of the cells were muscle fiber−like at passage 3 (Figure 6C). No contamination was observed. Depending on the injection requirements, sufficient amounts of pMDCs were prepared at passage 3.

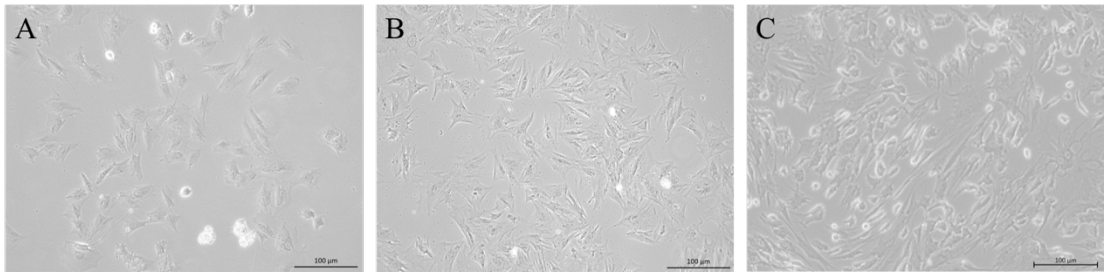

Figure 6: The morphology of pMDCs
Captured at passage 1 (A), 2 (B), 3 (C). pMDCs of passage 3 were used for injection experiments either in cadaveric samples or Living animals.

3.2 Characterization of pMDCs

3.2.1 The expression of muscle−specific markers by qRT−PCR

To characterize the pMDCs, the transcript expression of muscle−specific markers, including sMyoD1, sMyf 5, sMyf 6, sMSTN, sDesmin, sACT, Myl 1, was

determined by qRT−PCR. Three different cell sources of pMDCs were employed in this study: Cells from newborn WT boars, from newborn transgene−RPF^{+} boars, and from adult WT pigs were explored at marker gene expression levels to verify which population was appropriate for injection. The newborn WT cells were used as positive control[55]. As shown in Figure 7, all pMDCs from three cell sources expressed positively (high or low) several muscle−specific markers. The gene expressions of sMyf 5 in the newborn transgene−RFP^{+} was lower than other two groups. The expression of the sMSTN gene in the newborn transgene RFP^{+} group and adult WT group was lower compared to newborn WT group, indicating that pMDCs from these two group might have a higher proliferation potential. The result of lowest expression of sDesmin in the adult WT group convinced us to select this type cells for subsequent experiments not. No major differences in the other genes were observed between the three groups.

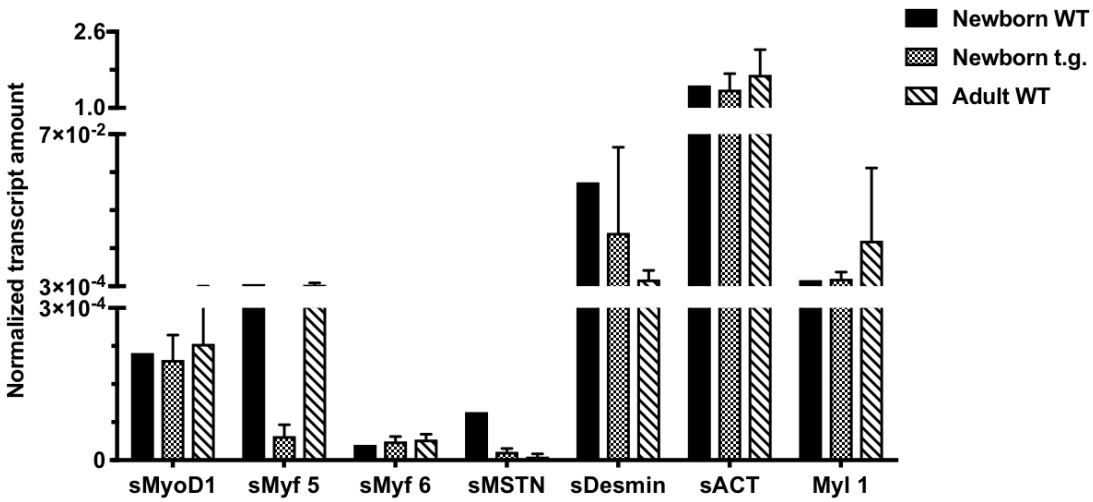

Figure 7: Detection of muscle−specific marker expression of pMDCs

Three different cell sources were detected at passage 2. pMDCs from newborn wild−type male pigs served as the positive control. There were no differences in expression of sMyoD1, sMyf6, sACT, and Myl1 transcripts, compared to the control group. The expression of sMyf5 in the newborn t.g. group was lower than in the control and adult WT groups. Both in newborn t.g. group and adult WT group MDCs had a lower expression of sMSTN compared to the controls.

3.2.2 The expression of Desmin, Fast myosin, and Slow myosin in pMDCs detected by immunofluorescence

To characterize the pMDCs on protein levels, the expression of myogenic makers Desmin, Fast myosin, and Slow myosin were detected by immunofluorescence (IF), respectively. staining omitting the primary antibody but using only the secondary antibody were used as controls (Figure 8). The results showed that the expression of Desmin and Fast myosin proteins in both, the newborn WT (Figure 8 A1, A3) and newborn t.g. groups (Figure 8 B1, B3), were higher compared to weak expression in adult WT cells (Figure 8 C1, C3). All of the three groups were negative for Slow myosin (Figure 8 A5, B5, C5). Compared to Fast myosin (Figure 8 A3, B3), the distribution of Desmin protein was not morphologically uniform in both of the newborn WT (Figure 8 A1) and t.g. group (Figure 8 B1), which may be caused by the pMDCs at various stages of myogenic differentiation. Thus, the pMDCs from newborn WT and newborn t.g. group were selected for subsequent cell injection experiments.

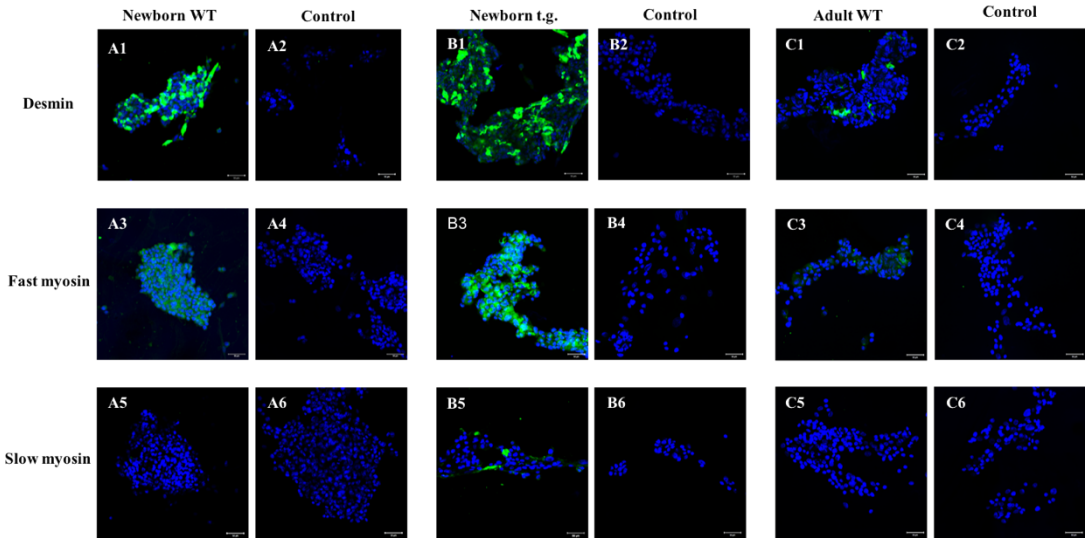

Figure 8: Expression of muscle−specific markers of pMDCs by IF

Three different cell sources were detected. Desmin and Fast myosin were highly expressed in the newborn WT (A1, A3) and newborn t.g. (B1, B3) group, but weakly expressed in adult WT group (C1, C3). Slow myosin was low expressed in all three groups (A5, B5, C5). pMDCs from newborn male pigs, whether transgenic or WT, were used for the injection in both CS and LA.

3.3 The survival of pMDCs that retrieved after injection by WaterJet E_{60-10} or William's Needle into the cadaveric samples

To examine the survival of Calcein AM−labeled pMDCs after injection in CS, the samples (n = 4) in each injection group were used for cell extraction by a syringe immediately after injection by WJ E_{60-10} and WN. Figure 9 shows an example of pMDCs from both, the WJ E_{60-10} (Figure 9 A) and WN injection group (Figure 9 B) after 5 days culture. Uninjected cells served as controls (Figure 9 C). Almost all the cells in both injection groups had intact cell membranes under the microscope and fluorescence staining to prove that they were the injected cells. There were no major differences between the injection groups (Figure 9 A3, B3) as well as the untreated group (Figure 9 C3), except the number of cells in the controls. We explain this difference by the incompleteness of cell extractions after cadaver tissue injections. The cells attachment to the culture vessel and the strong Calcein fluorescence of the labelled pMDCs suggested that the cells survived WJ E_{60-10} and WN injection in CS. However, the quality of the images was not high. Not all cytoplasmic fluorescence detected by dark−field fluorescence imaging (Figure 9 bottom panel) could be match up with the cells photographed by transmitted light mode (Figure 9 top panel). This was caused by the synthetic images generated by combining the transmitted light and immunofluorescence images using ImageJ software.

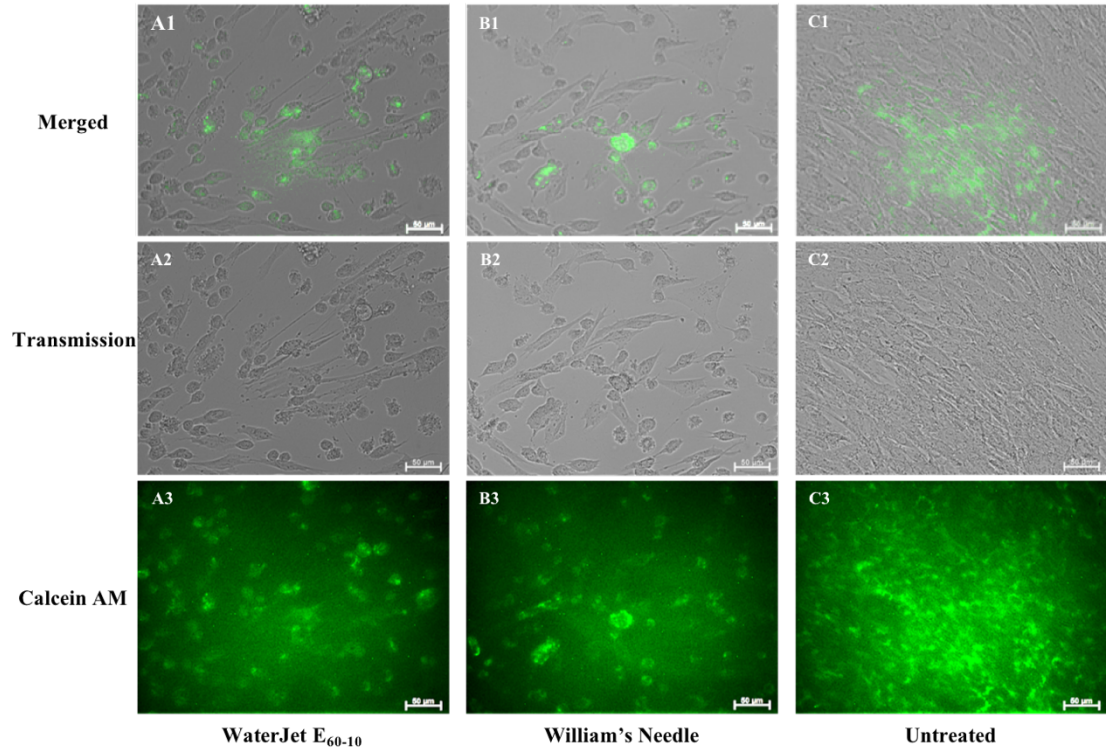

Figure 9: The survival of pMDCs after injected in cadaveric samples

With Calcein AM staining, cells were extracted after injection by WaterJet E60−10 and William's Needle by 18G hypodermic needle and syringe. The extracted cells were cultured in separate wells for 5 days. Cells without injection served as control (C1). By careful comparing the green fluorescent images (A3, B3, C3) with the transmission micrographs (A2, B2, C2), there was no difference between the three groups, and most of the cells remained intact. This demonstrated that pMDCs stained with Calcein AM can survived after injection in cadaveric sample with WaterJet E60−10 or William's Needle.

3.4 Location of pMDCs after William's Needle injection in cadaveric samples by IVIS

To visualize the location of pMDCs after WN injection in urethral tissue samples, the CS, including bladder and urethra, were analyzed by IVIS imaging (Figure 10). As fluorescence reference and to estimate the florescence intensities produced by defined number of labeled cells, serial dilutions of pMDCs were seeded in wells B1 (10^4 cells/well) to F1 (100 cells/well) in the 96−well plate. At the same time this served as a brightness scale for IVIS fluorescence setting (Figure 10 A). The data

indicated that IVIS imaging was sensitive enough to detect Calcein AM−labeled of no less than 10^4 pMDCs before injection into the tissue. However, the same setting was not appropriate for the MDC detection after injection into the tissue. As Figure 10 A shows, there were strong signal interferences throughout the bladder surface and parts of the urethra, making it impossible to distinguish the cell injection boundaries from autofluorescence signals. The main reason for this was the higher concentration of injected cells. For WN injection in CS, each time 3×10^4 pMDCs were injected into the urethra and bladder both at a superficial and deeper level. After adjusting the settings of the IVIS, only the superficial urethra injection site was recorded with exact location and boundaries of the cells applied (Figure 10 B). The yellow dots indicated a high concentration cells cluster, which was the centre of the injected cells. The low concentration of cells in red indicates the overall range and distribution of injected pMDCs. Then the segment of urethra with injected cells was precisely cut out and immediately stored in liquid nitrogen for later analysis by histology. The IVIS technique allowed us to identify and isolate the target area very quickly and accurately from the entire urethra.

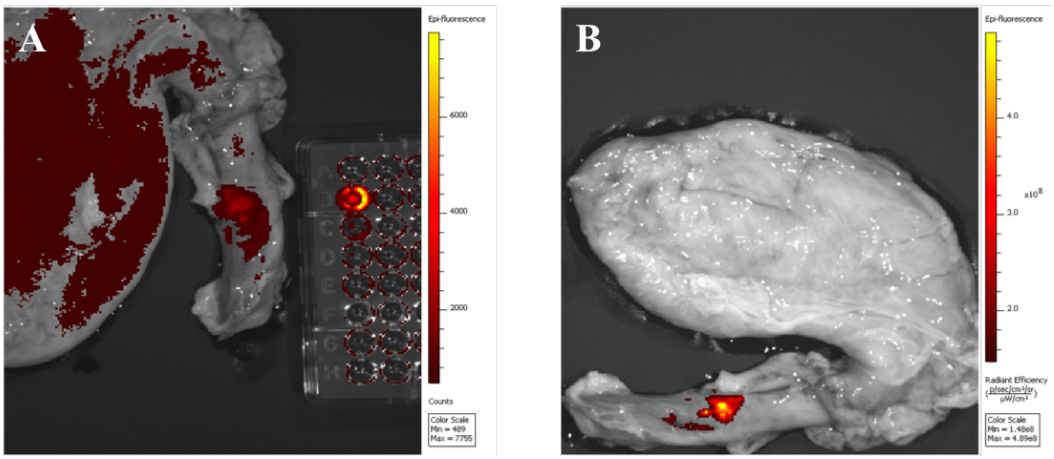

Figure 10: Location of pMDCs after William's Needle injection in cadaveric tissue by IVIS
(A) The 96−well culture plate with serial dilutions of labelled cells ranging from top B1 (104 cells/well) to bottom F1 (100 cells/well) was used as a brightness scale. 104 labelled cells can be easily detected. (B) After adjusting the settings, only cells stained with Calcein AM injected into the urethral surface were detected with the exact location and boundaries.

3.5 Localization and distribution of either t.g. RFP^+ or Calcein AM−labeled pMDCs after William's Needle injection vs WaterJet $E_{60–10}$ in cadaveric porcine urethra

To assess how the pMDCs were distributed by either WN or WJ $E_{60–10}$ injection in CS, cryosections (n = 11) were generated from the area determined by IVIS and analysed by aid of a fluorescence microscope. From the first layer of appearance of injected pMDCs to the last one including the maximum layer, micrographs were captured by Axiovert 200M microscope. The number of layers containing fluorescent cells was recoded to calculate distribution of the cells in the tissue. The distribution was referred to as Z−height in the samples. In the t.g. RFP^+ group, the whole tissue from maximum layer by WN (Figure 11 A1) and WJ $E_{60–10}$ (Figure 11 C1), scanned by LSM 510 after phalloindin staining, showed that pMDCs were enriched at the mucosa and submucosa layers of the urethra. Fluorescence stained rhabdosphincter samples were used for subsequent DISIC measurements. The injected pMDCs from t.g group (n = 7) could be identified with yellow fluorescence (Figure 11 A2, C2) combined from expression of the transgenic red fluorescent protein (iRFP 720) and the green fluorescence of phalloindin binding to muscle cells. A single large, dense mass of cells from t.g. group (n = 3) (Figure 11 A2) or multiple dense cell clusters with Calcein AM−labelled from WT group (n = 2) (Figure 11 B) were observed in the WN group. The cells injected by WJ $E_{60–10}$ showed a different, larger and more evenly distribution, combined with shallow centre of high cell density and a deep scattering distribution in t.g. group (n = 4) (Figure 11 C2) and WT group (n = 2) (Figure 11 D). Injected cells with intact membranes were observed in all immunofluorescence images. All nuclei were stained blue by DAPI. These results indicated that the fluorescence labelled pMDCs survived after WJ $E_{60–10}$ vs WN

injection in the CS. This motivated us to prepare the next steps, the in vivo experiments.

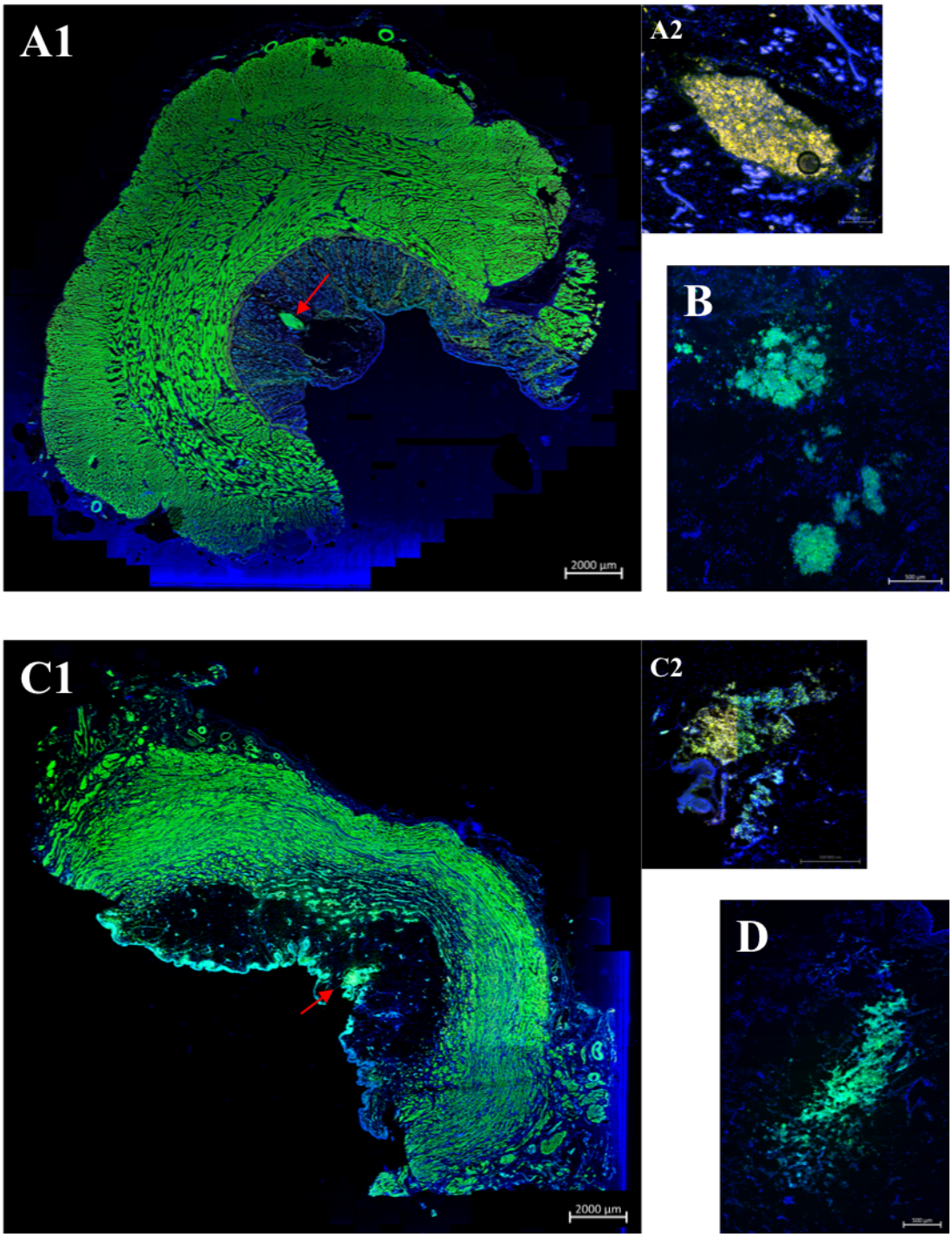

Figure 11: Localization and distribution of pMDCs after William's Needle or WaterJet E60−10 injection by LSM 510

By WN (A1) or WJ E60−10 (C1) injection, t.g. RFP^{+} pMDCs were located within the mucosa and submucosa layer, some distance from the muscle layer which was the treatment position. The cells

injected by WJ E60−10 showed a different, larger and more uniform distribution instead of a single large dense cell mass (A2) or multiple dense cell clusters of Calcein AM−labelled cells (B) by needle.

3.6 The success rate of the remaining uninjected pMDCs of BacMam vs PKH 26 stained after the living animal injection

To verify the survival of remaining uninjected pMDCs after in vivo surgery, half of which had been stained with BacMam GFP$^+$ while the other half with PKH 26, the cells were seeded in flasks and expanded for up to 5 days. Cells after 1 day of culture were observed and captured by Axiovert A1 Microscope (Figure 12). BacMam and PKH 26 staining can be detected in cell nucleus (Figure 12 C) and cytoplasm (Figure 12 D), respectively. Brightfield channel (Figure 12 B) was used as the reference of merged a picture. Most of the pMDCs was morphologically intact. By simply comparing in the merged picture (Figure 12 A) with the number of cells stained by BacMam or PKH 26 (Figure 12 C,D) we conclude that some cells did not show any fluorescence, and efficacy of BacMam−mediated fluorescence staining seemed clearly lower than the efficacy observed by PKH 26 staining (Figure 12).

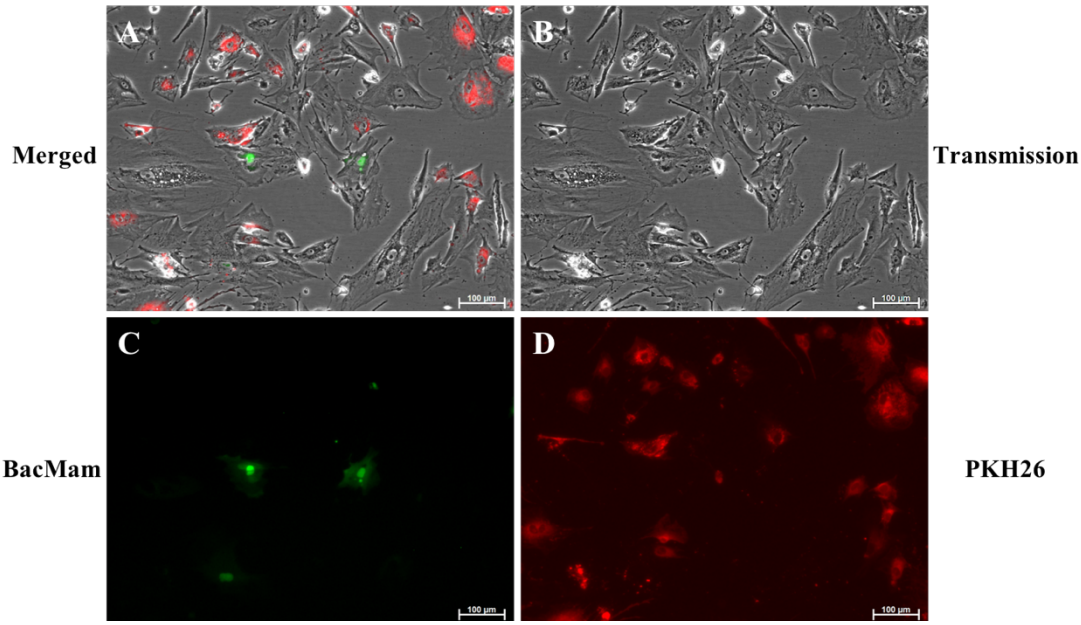

Figure 12: Survival rates and staining efficacy of the remaining uninjected pMDCs stained by BacMam vs PKH 26 one day after the injection

Half of the injected cells had been stained by BacMam expressing a GFP+ histone in the nucleus (C), the other half by PKH labelling of the cell membrane (D). The success rate of PKH 26 staining was higher than that of BacMam (A). Brightfield (B) used as the background of merged picture.

3.7 Urine diagnostics by Combur^{10} test M before WaterJet injection in living animal

Before urodynamic tests of the porcine urethral wall pressure – a surrogate to explore muscle strength on the sphincter complex − the health status of pig's urine was tested by Combur^{10} test M (Roche). The result showed that in 12 urine samples from pigs after WJ E_{60-10} injection and 7 day follow−up (n = 6) and E_{80-10} injections and 3 day follow−up (n = 6) no significant abnormalities were recorded. This indicated that at least there was no abnormality in the urinary system of these living pigs (*Table 12*). The normal range of SG is 1.010−1.025, normal pH: 5−6.6.

Table 12: Urine test before cell injection in living porcine urethra by Combur^{10} test M.

Combur^{10}−Test M	Animal	SG	pH	LEU	NIT	PRO	GLU	KET	UBG	BIL	ERY/Hb
E_{60-10} 7 day	M13	1.020	5	neg.	neg.	neg.	norm.	neg.	norm.	neg.	neg.
	M14	1.015	6	neg.	neg.	neg.	norm.	neg.	norm.	neg.	neg.
	M15	1.015	6	neg.	neg.	neg.	norm.	neg.	norm.	+	neg.
	M16	1.015	6	neg.	neg.	neg.	norm.	neg.	norm.	neg.	neg.
	M17	1.015	7	neg.	neg.	neg.	norm.	neg.	norm.	neg.	neg.
	M18	1.015	5	neg.	neg.	neg.	norm.	neg.	norm.	neg.	neg.
E_{80-10} 3 day	M19	1.020	6	neg.	neg.	neg.	norm.	neg.	norm.	neg.	neg.
	M20	1.015	5	neg.	neg.	neg.	norm.	neg.	norm.	neg.	neg.
	M21	1.015	6	neg.	neg.	neg.	norm.	neg.	norm.	neg.	neg.
	M22	1.015	6	neg.	neg.	neg.	norm.	neg.	norm.	2+	neg.
	M23	1.015	6	neg.	neg.	neg.	norm.	neg.	norm.	+	neg.
	M24	1.015	6	neg.	neg.	neg.	norm.	neg.	norm.	2+	neg.

3.8 Urodynamic test in living animals before Waterjet injection

To verify the location of continence zone at the urethra of each pig, the UPP include MUCP were measured before WJ injection (Figure 13). An older version the of Aquarius TT system with urodynamic catheter was employed for urodynamic

analyses of the WJ E_{60-10}, 30 min group (≙ day 1; n = 6) and 3 day group (n = 6). These analyses are named as test I. Due to technical difficulties with this device, the WJ E_{60-10}, 7 day group (n = 6) and the E_{80-10}, 7 day group (n = 6) were tested by a newer version of the same system (hardware and software!), and named test II. When comparing the results of the tests I and tests II with the two different versions, the urethral length in the test I series (89.10 ± 24.94 mm) was statistically significant longer (t = 5.90, P < 9.00E−06) than in the test II series (45.33 ± 6.01 mm). The continence zone in test I (48.00 ± 19.04 mm) was also statistically significant longer than in test II (34.25 ± 5.43 mm)(t = 2.40, P < 0.03). In contrast, there was no significant differences in MUCP between test I (94.20 ± 20.39 cmH_2O) and test II (104.92 ± 18.98 cm H_2O) (Figure 13). Thus, by detecting the continence zone and by determination of MUCP, the urethral sphincter muscle was accurately located for exact delivery pMDCs to the target in the female porcine urethra.

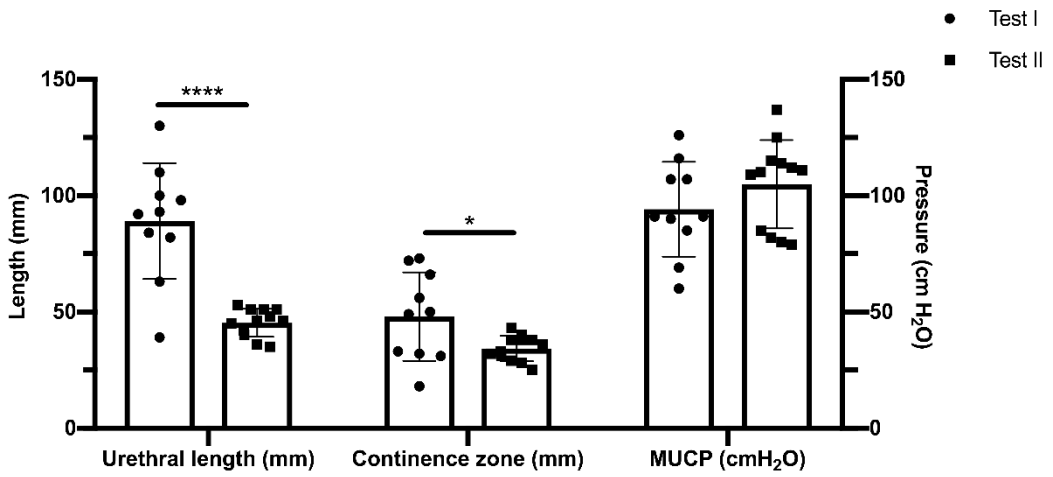

Figure 13: Determination of the urethral wall pressure in continence zone of living porcine urethrae The urodynamic measurements included urethral length, continence zone, and MUCP. The data were measured by an older instrument as Test I in WJ E_{60-10} 30 min and E_{60-10} 3 day group, or a more advanced instrument as Test II in WaterJet E_{60-10} 7 day and E_{80-10} 3 day group. Although there was a statistical difference in the length of urethra and continence zone between the new and old systems, we could still accurately locate the continence zone of each individual pig, thus achieving the purpose of determination of the injection zone.

3.9 Detection of BacMam vs PKH 26 labeled WT pMDCs by IVIS after WaterJet injection into living animal urethra

To localize the area of cell injection in the urethra after incubation and sacrifice of the pigs, the whole bladder and urethra were prepared, cooled on wet ice and scanned by IVIS with different appropriate settings for each fluorescent channel, i.e., green for BacMam− and red for PKH 26− labels and a false−color heat map was generated by the device based on signal intensities recorded in each channel (Figure 14). The yellow highlighted dot was the asymmetric center with a high cell density within the entire region containing injected pMDCs. The fluorescence center was closer to the distal ureteral opening, which was considered corresponding to the injection directions. From all the four animal groups treated, two injected regions could be observed in PKH 26 channel in 23/24 tissue samples (Figure 14 A1, B1, C1, D). The injected cells were detected at the same site in the BacMam channel with more sensitive settings of the IVIS. Only one site of the two injections with higher cell concentration (Figure 14 A2, C2) was observed by comparison with PKH 26 staining (Figure 14 A1, C1). Lower concentrations of injected cells were not detected by BacMam staining (Figure 14 A2, B2, C2). Based on the results of IVIS analyses of the whole urethra (Figure 14) versus fluorescence microscopy of cryosections (Figure 15) for the WJ E_{60-10} group, only PKH 26 staining was used further analyses of samples of the E_{80-10} 3 day group.

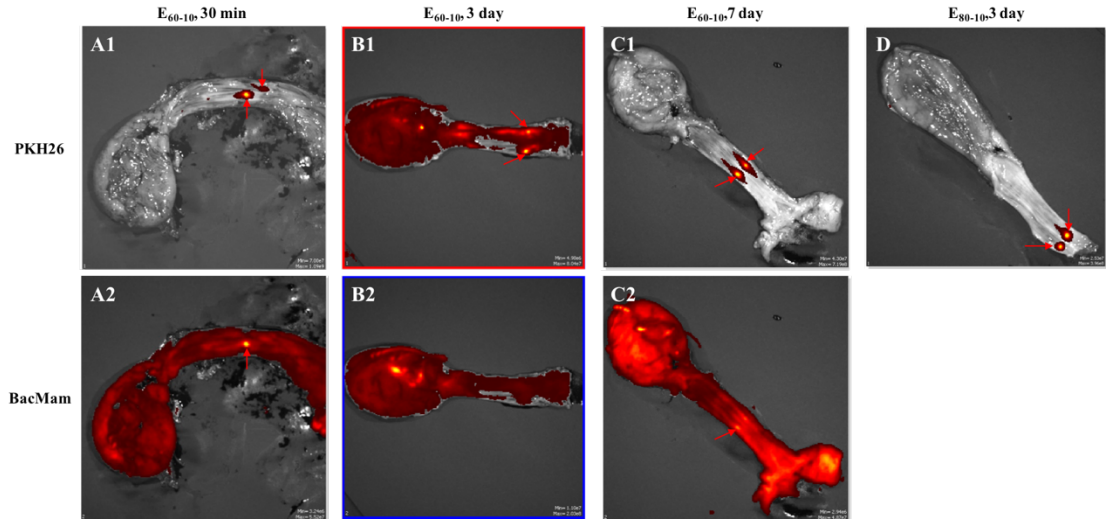

Figure 14: Localization of BacMam vs PKH 26−labelled pMDCs injected in porcine urethra by IVIS The red areas by arrows pointed (A1, B1, C1, D) were the location of twice injected PKH 26−labelled pMDCs in each animal. Clearly region of BacMam staining was detected in some of the tissue (A2). Others samples were somewhat more difficult to identify the region of the cell injection (B2, C2).

3.10 Localization and distribution of wild type pMDCs after WaterJet injection in living animals

To analyze the situation of WT pMDCs after WJ injection in the urethra of living pigs, the tile scan by fluorescence microscope (LSM 510, Zeiss) for maximum layer of each group (n = 23/23) from totally four groups were captured to verify the localization and distribution of injected cells (Figure 15 A ~ D). The harvest timing was chosen as 30 min, 3 and 7 days follow−up after WJ injection by E_{60-10} VS E_{80-10}. The injected pMDCs were delivered at submucosal layer of the urethra formed a cluster with high concentration in the centre. Every small picture was captured before phalloindin staining which enabled us to observe the morphology of injected cells with an intact membrane structure. These embedded images, which came from an upright microscope, were inverted for consistency with the larger image, with a scale of 100 µm for all images. In all the three groups from E_{60-10} (n = 17/18 animals) (Figure 15 A, B, C), There was no significant difference in cell morphology

and distribution. But when compared with E_{80-10} group (n = 6/6) (Figure 15 D), PKH 26−labelled cells of E_{60-10} group appeared closer to the targeted position, the lissosphincter and rhabdosphincter. All the panorama pictures with phalloindin staining were measured and analysed as shown later. In particular, there was one case in the E_{60-10} group (1/36) (Figure 15 E) in which the cells were fully reached the muscle layer without completely penetrating. Another special case showed a totally penetrated structure from the E_{80-10} group (2/12, injection sites) (Figure 15 F). In one of the two injections, only the damaged muscle structure could be detected at the injection site without any injection cells remaining, and in the other case, only a small amounts of cells remained in the urethra. Images of the entire tissue were taken from an inverted confocal laser microscope.

The statistical analysis of all the data was presented in the following sections.

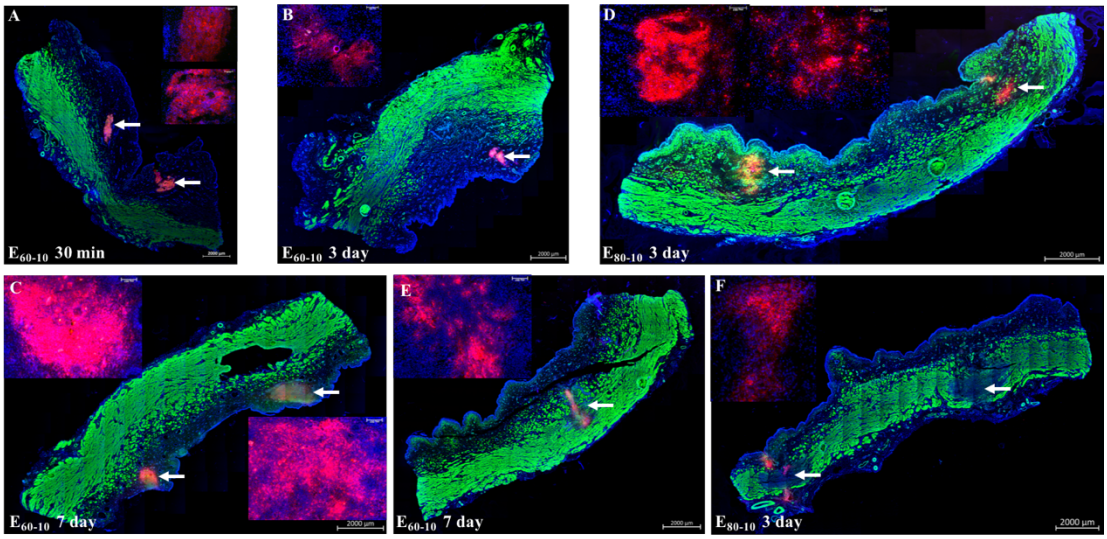

Figure 15: Localization and distribution of pMDCs by WaterJet injection in the urethra of living animals

In all groups intact appearing cells were observed by microscopy (A ~ F). Compared to the E_{60-10} group (A , B , C), the cells from the E_{80-10} group (D) were closer to the muscle layer, which was the therapeutic target. In one animal from the E_{60-10} 7 day group (E) injected cells reached the muscle layer without completely penetrating it. Another special case was that cells from one animal of the E_{80-10} 3 day group (F) totally penetrated the tissue.

3.11 Comparing the results of pMDCs injection by William's Needle vs WaterJet in cadaveric samples and living animals

To investigate the superiority of the new technology of WJ injection, the successful ratios of cell injection and survival rates of cells extracted after injection in both, in CS and LA, were calculate (*Table 13*). Each CS was injected one time. In the first CS step, t.g. RFP^+ cells (n = 13) were used for injecting in the urethra by the classic method WN (n = 5) vs new technology WJ $E_{60–10}$ (n = 8). Among them, the samples used for extraction were 2 cases in the WN group, 4 cases in the WJ $E_{60–10}$ group. For generation of cryosections, 3 samples were used in WN group and 4 samples in the WJ $E_{60–10}$ group.

In the second series of CS injections, Calcein AM−labelled WT pMDCs were injected by WN (n = 4) vs WJ $E_{60–10}$ (n = 8). In the WN group, half of the samples (n = 2) were set aside for extraction and culture of cells, and other half for preparation of cryosections. The same half to half ratio (n = 4 for each) was used in the WJ $E_{60–10}$ group.

Both the success rates of cell injection and the survival of cells extracted after injection by WN in CS were 100%. The survival rate in the WJ group was also 100%, but the success rate of cell injection was lower than 75% (6/8). In 2 samples from the t.g. RFP^+ group fluorescent cells were not detected by either Axiovert fluorescence microscope or LSM510. This indicated that the risk of cell loss after orthogonal cell injection by WJ was somewhat higher when compared to angulated cell injections by WN. The rather stiff bedding of the CS on a sponge and the thin urethral tissue may also facilitate cell loss after WJ injections.

In the LA series of investigations, injections by WJ $E_{60–10}$ (n = 18) and $E_{80–10}$ (n = 6), each animal was injected two times (n = 48 injections total) at the "3' and 9' clock positions", respectively. The injection success rate WJ injections in LA, as

determined by detection of fluorescent pMDCs in the urethra was 95.83% (46/48 injections in 24 pigs). Only in the sample from on animal with two cells injections from E_{60-10} 3 day group, PKH 26 stained cells remained undetectable by either IVIS or fluorescence microscopy. It is considered that the injected cells may be lost in an urethral segment not harvested properly. Cell survival rates in LA experiments could not be assessed in this study because in the in vivo experiments, when cells were injected into the urethra through endoscope, there was no way to perform cell extractions without injury of the tissue and consequent loss of cells due to inflammation or even premature abortion of the animal due to critical health conditions, Moreover, interventions during follow−up to obtain cell or tissue samples had not been approved by the local animal welfare authorities.

Table 13: The ratio of success injection by William's Needle and Waterjet.

Group	Tissue for cryosection	Injection time	Successful cell injection	Successful rate of cell injection	Survival rate of cells extracted after injection
WN in CS	5	5	5	100%	100% (4 / 4)
WJ in CS	8	8	6	75%	100% (8 / 8)
WJ in LA	24	48	46	95.83%	

3.12 Expression of pSRY gene DNA by PCR in cryosection from living animals

To verify the proper localization of fluorescent labelled pMDCs after WJ injection in the urethra of LA and to confirm intake chromosome DNA of the injected male cells, the DNA was isolated from 4−6 cryosections containing injected cells to detect the pSRY gene which located at male Y−chromosome by PCR. The PCR product was detected at 133bp of length (Figure 16) in WJ E_{60-10} 30 min (n = 6) (Figure 16 A), 3 day (n = 5/6) (Figure 16 B), 7 day (n = 6) (Figure 16 C) and E_{80-10} (n = 6) (Figure

16 D). DNA extracted from porcine male and female tissues served as positive and negative controls in each group.

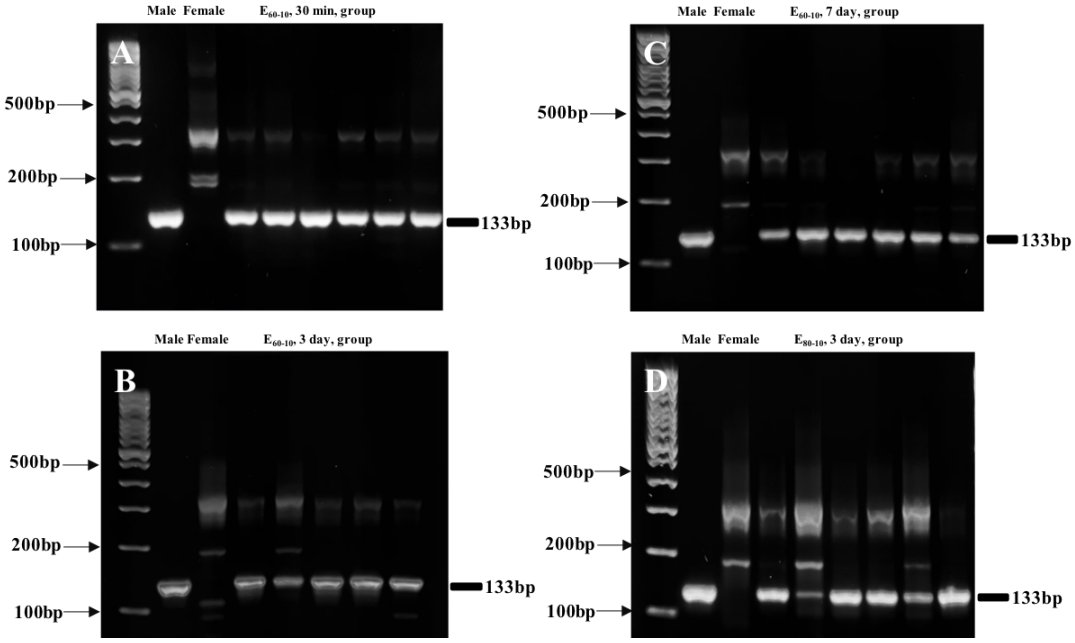

Figure 16: Detection of the pSRY gene in cryosection containing male pMDCs injected by WaterJet in female porcine urethrae

The products of pSRY gene amplification from different groups (A−D) were analyzed by agarose gel electrophoresis to confirm that products were located at 133bp as expected for the pSRY gene. Tissues from the male and female were used as positive and negative controls, respectively as indicated.

3.13 Quantitative analysis of XYZ−3D and DISIC of cell location and distribution in the urethra

To compare the localization and distribution of pMDCs after injection in either CS or LA by WN vs WJ, the quantitative measurements of XYZ−3D (including the length in one dimension and area in two dimensions) and DISIC from each group were recorded in the maximum layer from tile scans generated by LSM510 microscopy. Because effective intergroup comparisons can only occur for single factor changes, the groups were compared as WJ E_{80-10}−LA vs WJ E_{60-10}−LA, WJ E_{60-10}−LA vs WJ E_{60-10}−CS, WJ E_{60-10}−CS vs WN−CS (Figure 17).

In the first series of analyses (Figure 17 A), X−depth, Y−width and Z−height of injected cells clusters were measured in one dimension. X−depth of WJ $E_{60–10}$−LA (1459 ± 528.1 µm) was statistically significant shorter (t = 4.34, P = 0.0001) than WJ $E_{60–10}$−CS (2487 ± 577.4 µm). Y−width of WJ $E_{80–10}$−LA (1453 ± 755.4 µm) was statistically significant wider (t = 2.035, P = 0.0479) than WJ $E_{60–10}$−LA (1020 ± 587 µm). The Z−height of WJ $E_{60–10}$−CS group (2001 ± 1018 µm) was statistically significant shorter (t = 4.292, P = 0.002) than that of WN group (5684 ± 1795 µm). The Z−height of WJ $E_{60–10}$−LA group (7740 ± 3297 µm) was statistically significant longer (t = 4.292, P = 0.002) than that of WJ $E_{60–10}$−CS group. The Z−height of WJ $E_{80–10}$−LA group (13250 ± 3931 µm) was statistically significant longer (t = 4.734, P < 0.0001) than that of WJ $E_{60–10}$−LA group, which caused by the higher pressure of first phase of WJ injection.

In the second series of experiments (Figure 17 B), the areas of XY, YZ and XZ were calculated and compared in two dimensions. There was no difference between all the groups in XY. The YZ of WJ $E_{80–10}$−LA group (1.99E+07 ± 1.21E+07 µm) was statistically significant bigger (t = 3.775, P = 0.0005) than that of WJ $E_{60–10}$−LA group (8.52E+06 ± 7.66E+06 µm). The XZ of WJ $E_{60–10}$−LA group (1.15E+07 ± 6.66E+06 µm) was statistically significant bigger (t = 2.42, P = 0.0204) than that of WJ $E_{60–10}$−CS group (4.79E+06 ± 2.48E+06 µm). The XZ of WJ $E_{80–10}$−LA group (1.90E+07 ± 1.35E+07 µm) was statistically significant bigger (t = 2.517, P = 0.0156) than that of WJ $E_{60–10}$−LA group.

In addition, the DISIC of WJ $E_{80–10}$−LA injections (879.81 ± 316.69 µm) was compared to WJ $E_{60–10}$−LA injections (2271.14 ± 876.51 µm) (Figure 17 C). Determining the DISIC yielded a statistically significant decreased distance between the sphincter muscle layer and the centre of the cell injection (t = 5.12, P < 0.0001). This is clear evidence that injection depths can be adapted to the tissue targeted and the clinical needs by preselection of the distinct pressure profiles. A

higher penetration pressures grants deeper penetration of cells applied in tissues targeted.

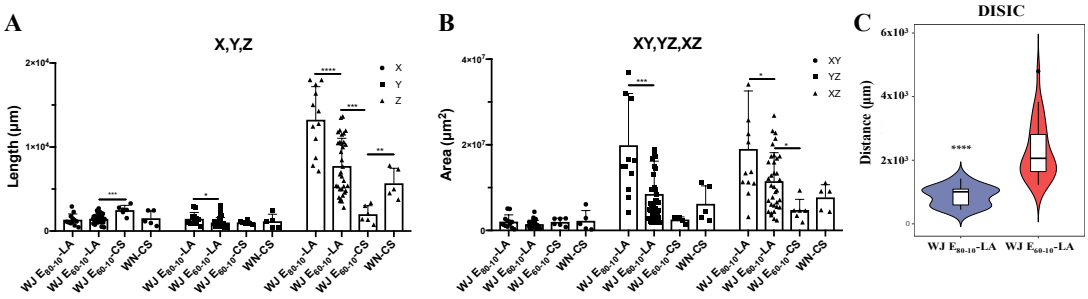

Figure 17: Quantitative analysis of XYZ−3D and DISIC of cell location and distribution in the urethra of LA

The distance comparison with E_{60-10} group showed that the Y and Z axes in E_{80-10} group were statistically significant wider except for the X axis (A). In the area comparison of the three dimensions, the E_{80-10} group was also statistically significant larger than E_{60-10} injected animals (B). This suggested that by WaterJet E_{80-10}, cells could be sprayed into the urethra in a more distributed way. DISIC analyses showed that the E_{80-10} injected cells statistically significant closer to rhabdosphincter (C), potentially indicating that the E_{80-10} pressure might be a more suitable choice to transport cells into the urethra as therapeutic aim.

3.14 HE & Azan staining on cryosections of cadaveric samples and living animals by William's Needle vs WaterJet (E_{60-10} or E_{80-10})

To investigate the change of muscle structure and distribution of the injected cells, adjacent cryosections for immunofluorescence detection (match with Figure 11 and Figure 15) were used for HE (1) & Azan staining (2) for every sample (Figure 18). In the HE staining of cryosections, the cell nucleus presents as blue and the cytoplasm as reddish stain. In the Azan staining samples, the nucleus as red stain, the cytoplasm and muscle tissue as reddish/violet, and connective tissue fibers such as collagen and reticular structures as blue colour. One or both of the injected sites from urethra samples were recorded with 10x magnification, which from each sample chosen from every group, are shown together (Figure 18). No areas of tissue necrosis was observed in cryosections in any of the tissues investigated. The injected cells had

intact nuclei and membranes. However, in samples from one injection cells were attached to the target muscle layer in animals from WJ $E_{60–10}$ 7 day group (Figure 18 E1, E2) and in another animal, cells totally penetrated after WJ $E_{80–10}$ injection in the 3 day follow−up group (Figure 18 F1, F2). In general, the injected pMDCs were located in the submucosa, which corroborated the results obtained by fluorescence microscopy. In contrast, a large cavitation with no obvious channel was observed only in the WN−CS group (Figure 18 A1, A2), which was caused by the injection fluid. In the WJ−CS or LA group, a tunnel from the urethral epithelium to the site of the injected cells can be clearly detected, which was formed by the first phase of WJ injection (Figure 18 B1, B2, C1, C2, D1, D2). There was no significant differences in tunnel sizes when samples from the different tissues and pressures were compared. The DISIC of WJ $E_{80–10}$ group was closer to the sphincter muscle than in the $E_{60–10}$ group, which was also supported by statistical results of fluorescence microscopy (Figure 17 C). Cracks in the strips appeared in WJ $E_{60–10}$ 30 min in LA (Figure 18 C) and WJ $E_{60–10}$ 7 day in LA (Figure 18 E) as well as tissue overlap in WJ $E_{80–10}$ 3 day in LA, which was considered an artefact most likely due to too fast temperature drop in a short time when preparing cryosection and/or by storage of the porcine tissue samples in liquid nitrogen.

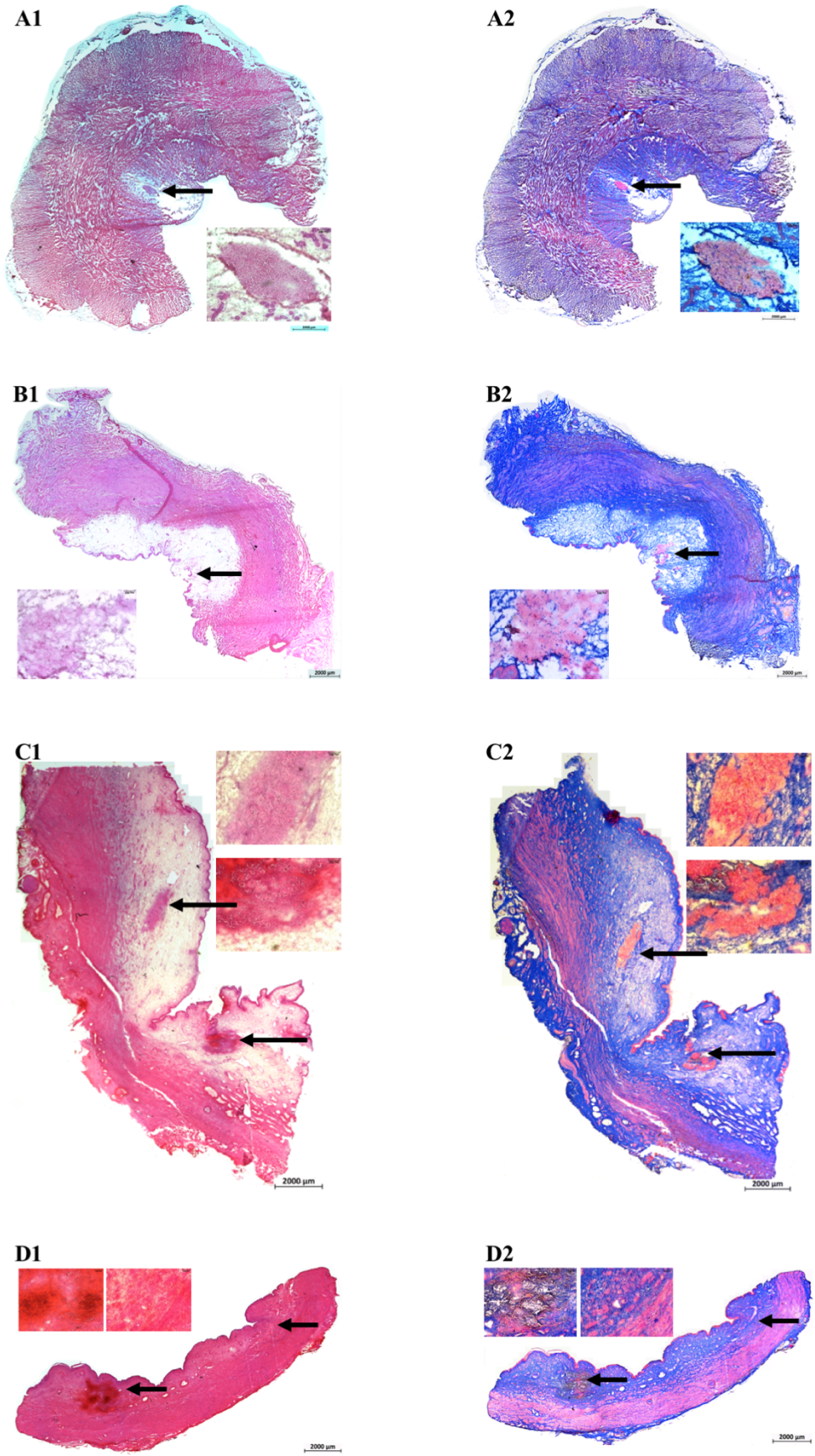
A1
A2
B1
B2
C1
C2
D1
D2
2000 µm

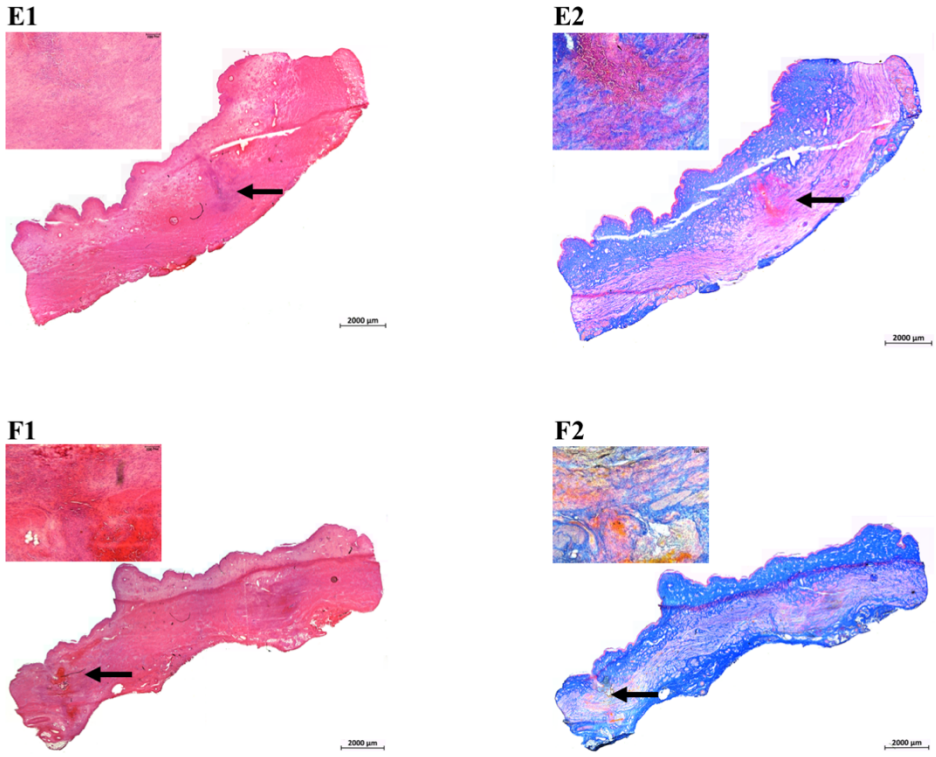

Figure 18: HE & Azan staining on Cadaveric samples and Living animals by William's Needle vs WaterJet

In the figure, 1 represented HE staining and 2 represented Azan staining. (A) WN in CS. (B) WJ E_{60-10} in CS. (C) WJ E_{60-10} 30 min in LA. (D) WJ E_{80-10} 3 day in LA. (E) WJ E_{60-10} 7 day in LA, attach muscle layer. (F) WJ E_{80-10} 3 day in LA, totally penetrated.

4 Discussion

Treatment of stress urinary incontinence by cell therapies to regenerate the function of urethrae sphincter is gaining considerable interest in recent years. In pre−clinical animal studies and clinical studies using multiples type of autologous cells were employed. Although surgery−based procedures including sling procedure, which is the gold standard right now, and bulking agent injection could maintain or re−establish continence by enhancing support function of the pelvic floor, the intrinsic function of urethral sphincter was not repaired by these therapies. Thus, cell therapy could become the key to restore the physiological closure function of the urethral sphincter complex. Moreover, a high ratio up to 20% patients reported persisting incontinence after surgery and needed additional surgery[61]. Other side effects, such as urinary tract infection and erosion, were also reported frequently[62]. While cell therapy has not become a standard clinical treatment so far, in many different studies employing animal models of SUI, cell therapies granted a positive outcome[35, 63]. In the early days of animal experimentation, the mouse was used as the animal model in most experiments. Then, however, multiple animal models emerged, including rabbit, dog and pig[35]. Unfortunately, in many studies control groups, standardized procedures, or meaningful long−term follow−up are missing. This leads to variable outcome and inconsistent assessment. In recent years, clinical feasibility trials were not worthy of attention due to the injection of uncontrollable fully penetration[64]. However, one recent meta−analysis reported that, in vitro expanded myoblast could be an alternative providing greater effect with lower risk of side effect, less invasiveness and higher costs when compared to Midurethral slings for surgery[65]. The further development of the technologies for SUI treatment by in vitro expanded myoblast could reduce the costs and increase the efficacy of such therapies at the same time. Other studies reported that the injection of the

chemokine CXCL 12, or the application of exosomes of the secretum of regenerative cells could also be a promising alternative or complementary treatment to cell therapy to reconstruct the structure of the urinary sphincter[36]. But acting only a limited time is the disadvantage of these non−cell therapies. Such reagents will be absorbed rapidly after injection by cells or by extracellular matrix components in the area of injection. While the concentration of such active compounds after injection is difficult to ensure, they may in addition be easily diluted by physiological fluids, including the lymph. As the tissue targeted by cell injection moves during voiding, fluids are more likely to deviate at the chosen treatment site than cells, further speeding up processes of dilution and thus reducing therapeutic effectiveness. Moreover, invasive therapies may cause even minor local inflammations, including infiltration of mononuclear cells. This may reduce the availability of the soluble regenerative factors as well e.g., by proteases secreted during inflammation. Therefore, we investigated a novel, rapid, simplified and less invasive transurethral cell injection technique based on a novel WaterJet technology to improve the effectiveness of cell therapy of stress urinary incontinence.

In our research, we aimed at two challenges of cell therapy, the delivery route and cell distribution. Further challenges of SUI cell therapies include the isolation, characterization, and large−scale expansion of the regenerative cells, production of cells with the features needed, robust animal models of urinary incontinence, adaptation of the optimal volume of injected cells to the tissue targeted, and others. Some of these challenges were already explored to some extent[66]. In a previous study, Yokoyama and colleagues confirmed that the autologous MDCs could survive for 30 days in situ after injection for tissue regeneration of stress urinary incontinence[67]. This suggests the feasibility of long−term regeneration therapy with MDCs. However, only approximately 50% implanted smooth muscle cells were detected 1 hour after injection by needle in the heart muscle. Additionally, no

cells were detectable 1 week after injection. This may be explained with ischemic injury of the muscle tissue through the injection needle[68]. To prevent a huge amount of cell loss early after injection, biomaterials such as injectable hydrogels or microbeads could provide domains for cell attachment and help to prevent cell draining though the injection canal[69-71]. Improving the route and precision of cell injection is the key to reduce the loss of cells and achieve minimal injection damage. In recent studies, needle injections were explored comparing a transurethral, a transperineal or periurethral application[72]. Our recent pre−clinical study included about 100 Göttingen minipigs and documented that only in about 45% of animals cells injected by needle and transurethral cystoscopy under visual control were detected in the sphincter muscle[49, 73]. But all of these methods used a needle for cell injection. Recently, a novel needle−free technique WaterJet was designed to gently deliver mesenchymal stromal cells to the urethral sphincter under cystoscope[52]. The results show that MSCs injected into culture medium by WaterJet was equal or even better in the yield compared to needle. This technology provided fast and precise cell delivery to the targeted submucosal layers besides the sphincter muscle. A modified Erbejet2 prototype with two−phase design was used for cell transplantation in this study, which ensures a high pressure for stable, fast and accurate tissue penetration to the targeted location, as well as a rapid switch to low pressure for cell delivery with high cell viability by reducing the shear stress[52, 53]. With appropriate pressure levels, loss of large amounts of cells and full penetration of the delicate sphincter muscle was avoided. Moreover, recent research reported that the cell survival rates of slow flow by needle injection decreased the viability of cell delivery and increased the apoptosis within 2 days[73]. This conclusion supported shortening cell contact time is more advantageous for any narrow injection devices, which attain is in favour of the two−phased WJ

technology with such a rapid transportation speed and contact time of cells in the injection device.

In this project, we further explored the performance of the delivery of porcine MDCs by the novel WaterJet injection method both, in cadaveric samples and in vivo in living pigs. Injections by WN and not−injected cells served as controls. Although the condition of injection in cadaveric tissue is not exactly comparable to that in vivo, testing the appropriate injection pressure for viable MDCs without full penetration and demonstrating the distribution of cells in the tissue targeted was necessary and economic. Therefore, fresh porcine cadaveric tissues of the urethral sphincter were prepared and utilized to inject fluorescence−stained MDCs by WaterJet vs needle. By this we aimed to mimic the clinical situation to verify the feasibility. As presented in the section Materials and Method in figure 1, both WJ E_{60-10} and WN injection generated a bubble in cadaveric tissue, the dome of which was 2−3 mm wide and 3−4 mm high. It is difficult to detect the exact survival rate of cells after injection, as direct viability measures of cells injected in cadaveric urethra samples were biased by cells that were not injected in the tissue but remained on its surface. However, sealing the samples immediately after injection by a so−called super glue, followed by rinsing the samples, reduced the contamination of cells attached to the tissue surface only. For enumeration of cell viabilities by WJ versus WN injections, cells were isolated from the tissue, counted, and incubated and expanded for up to 5 days. This documented that the number of viable MDCs retrieved after WJ injection were comparable to the WN injection group corroborating the earlier studies with stroma cells[52, 53]. Moreover, cell viabilities were confirmed by staining the cells with Calcein-AM. Thus, viable cells appeared in green fluorescence upon injection in cadaveric samples followed by extraction and expansion for a few days. However, after WJ injection in CS, MDCs were not found dispersed in all the area injected but only one huge or a few large

and dense cell clusters at the centre of the bubble. We hypothesize that this is a result of shaking in the hand during the injection or the withdrawal process. This artefact also may be caused by the tissue stiffness, which impulse injected cells from tissue to the centre of bubble. The injection with nano− and microparticles yielded patterns with the same distribution[52, 74, 75]. Instead of high−density cell clusters, MDCs were formed as a "spray fan" shape of evenly distribution after a two−phase WJ $E_{60–10}$ injection process in cadaveric tissue. The moderate pressure E_{60} opened the canals by injecting a small amount of PBS liquid to the mucosal or submucosal layer while avoiding full penetration out of muscle layer. The form of WJ injection is a direct cause of the "spray fan" cell distribution. After opening the tissue by the E_{60} or E_{80} pressure, within milliseconds a reduced pressure is applied to gently transfer the MDCs at E_{10} in these micro−cavities and thus maintaining a high cell viability. The injected MDCs were observed evenly distributed from the narrow inlet at the epithelial layer of the urethra to the broad distribution at submucosal layer. Most of the cells were located near the centre of the distribution. Scattered cells lined the tail of the fan. Seldom cells were found near the entry side close to the epithelial layer due to the decrease pressure of WaterJet and closing tissue channels to compress cells out ward.

To quantify and compare the distribution of cells after WJ vs needle injections, the length of X−depth, Y−width and Z−height were measured from stacks of consecutive microscopical pictures of fluorescent cells within the maximum cell injection area. In the process of collecting the cell distribution data, we realized that the different injection angles of WJ and WN lead to the completely opposite meanings of X−depth and Z−height on the sagittal plane. Therefore, as a remedial alternative, X− and Z− measurements from the WJ data sets of cadaver injections were exchanged. Further consideration should be given to injecting into a more realistic urethral environment in possible future experiments with cadaveric

specimens. Compared to angulated WJ injection, the Z−height of orthogonal WN group was statically significant longer, which probably may be associated with higher pressure at the injection direction from the elongated needle. This also lead to a more even distribution of injected cells in the WJ group in all the three directions and explained the shorter X−depth of the WN group. The second reason was, MDCs may flow back out from the WN injection canal since the fluid pressure of the injection dome and eventually formed a narrow spindle distribution in the sagittal plane.

Considering the moderate success rates by WN application achieved in the previous in vivo trials[49] in this study at least comparable cohort sizes of 6 animals per injection group and at least 4 animals in not−injected control groups were computed to reach statistical significance. This cohort size of 6 pigs applied for each follow−up scheme as well. Therefore, animals injected by WJ E_{60-10} injection with MDCs were observed over 3 different periods of follow−up to observe the continuity of cell survival and distribution. Studies performed in parallel to this thesis by others provide evidence that fluids could not get though the urothelial layer by a pressure below E_{40}, and fluids were lost by penetration of the whole urethra in the CS by a pressure above E_{80}[74, 75]. Hence, in this study pressure levels of E_{60} and E_{80} were chosen for tissue opening, and E_{10} was employed to apply the cells, of course. An elevated pressure E_{80-10} with 3 day follow−up was set up to test as a more appropriate choice for cell transplantation closer to urinary sphincter muscle. Technically, it was hard to retrieving injected cells directly after in vivo injection, as the total numbers of animals granted had to be limited due to the 3R consideration. Injection and immediate retrieval experiments were only performed with porcine cadaveric tissue samples. But such in vivo injection− immediate cell harvest analyses may be required if the procedures will be developed for clinical feasibility studies and first−in−man human trials. In this thesis the rest of uninjected

fluorescence staining MDCs was counted, seeded and culture again for 1 – 2 days again to at least gain hints if the cells were viable immediately prior to injection in animals. Our data indicated that the remaining fluorescent cells were highly viable (95% by trypan blue dye exclusion counting in a haematocytometer; data not shown) even after several hours of lasting at ambient temperature in injection medium in the animal surgery theatre.

Another aspect must be considered as well. The ratio of fluorescence staining and the proportion of the injected cells that are stained may suggest that the success rate of BacMam staining was much lower than that of PKH 26. This result also suggested that PKH 26 would play a more important role in cell tracing of in vivo experiments, combined with the strong penetrating characteristics of red spectrum, which is the key to tissues. Moreover, all the animals investigated underwent urine diagnostics to show no abnormalities in the urinary system or infections prior to surgery. Urine tests were performed by Combur^{10} test M sticks and no significant abnormalities were noted in this study. In addition, to localize the urethral sphincter muscle for cell injection at optimal sides, urodynamic measurement of the wall pressure of the porcine urethra was performed. However, due to hardware and software incompatibilities, two different versions of Aquarius TT urodynamic measurement had to be employed, and different results were obtained. Since the same breed of pigs, same age, size, weight characteristics, and animals from the same breeder were used in all the in vivo studies, both the significant differences in the functional length of the urethra as well as the differences in the continence zone detected by the two versions of Aquarius TT were attributed to the different version of the machine and software. However, these differences were not the main goals of this study. But the target MUCP zone of every pig was located accurately for delivery of pMDCs, because there was no difference in MUCP between the two versions employed.

During the WJ injection small urethral bleeding was observed in vivo by cystoscope. Formation of hematoma was observed in the tissue samples in less than half of the animals. But the bleeding was transient because of the spontaneous closing of small WJ injection canal and the hematoma was seen only in pigs with a follow−up of a few hours to three days. The hematoma resolved completely in animals harvested after one week of follow−up. Moreover, in comparison to other animal SUI studies, this study improved in an important aspect as well. The MPCs were isolated from male litter mates of the female pigs which were raised for cell injections. These brother−sister injections had to the best of my knowledge not been performed in the context of SUI research and therefore present a novelty. Immune suppression to avoid rejection of injected cells was not required. This protocol comes therefore closer to the clinical situation of a autologous cell therapy than previous studies and at the same time facilitates the detection of the injected cells after follow−up e.g., by detection of the Y−chromosome and genes located on it. Of note, without any immune suppressive treatment, like ciclosporin and corticosteroids, infiltration of mononuclear cells including neutrophils were not detected one week after injection[76]. Therefore, we concluded that cell therapy of the urethra by a WJ technique caused only very minor damage to tissue. At the same time, the short wound opening time and rapid self−healing period tend to leave the injection site and urethra intact, thus avoiding urine and possible bacterial infection. Several articles explored these advantages by this novel WJ technology at gastrointestinal with self−sealing of epithelia and submucosal tissues[77-79]. The cell distribution by WJ application was measured exactly as in cadaveric samples. In both the cadaveric specimens and in vivo experiments, there were multiple factor changes among the groups. So we only compared the groups with single factor changes in pairs. The significant differences in X−depth between WJ E_{60-10}−LA vs. WJ E_{60-10}−CS may be in part explained by differences in tissue elasticity and higher mobility in vivo.

The significant wider Y−width of WJ E_{80-10}−LA compared to WJ E_{60-10}−LA may due to the higher pressure of first phase of WJ expanding more spaces in the urethra. The longer Z−height of WJ E_{60-10}−LA compare to WJ E_{60-10}−CS group could be explained that X and Z axis shared the power of the injection so that their lengths were inversely proportional. In order to further reveal the cell distribution, the areas in three dimensions were calculated. The larger YZ− of WJ E_{80-10}−LA compared to WJ E_{60-10}−LA indicated that the distribution of injected cells of WJ E_{80-10}−LA group was more even in 2D dimension paralleled to rhabdosphincter. The lager XZ− of WJ E_{60-10}−LA compared to WJ E_{60-10}−CS may due to the tissue resistance in dead specimens was higher than that in vivo. The bigger XZ− of WJ E_{80-10}−LA compared to WJ E_{60-10}−LA suggested that the higher pressure at the first phase of WJ can deliver the cells more evenly distributed along the injection direction. At last, the decreased length of DISIC of WJ E_{80-10} verified that injected cells were closer to the targeted rhabdosphincter in vivo, compared to WJ E_{60-10}−LA.

Besides analysis of the cell distribution, the success rate of cell injection were also vital links to improve cell therapy. As briefly mentioned above, upon injection of cells by transurethral route and WN in female pigs, in nearly 50% of animals investigated cells were misplaces[49, 80]. In other studies, accurate cell delivery to the external urethral sphincter was limited to 67% by needle injection. This insufficient rate of delivery as well as leakage of cell suspension (19%) was the disadvantage of needle injections[50]. In contrast, in our study, labelled pMDCs were detected in the urethra of 95% pigs investigated (n = 23/24) by IVIS scanning of tissue samples as well as in the corresponding cryosections after WJ injection. The missing one out of the 24 animals was considered as deficiency of the urethral segment containing the injected pMDCs due to the maloperation of tissue harvesting. The IVIS analyses indicated in addition, that PKH 26 is the more efficient as tracer fluorescent marker for IVIS when compared to other labels used

in this thesis. Moreover, the full penetration was found in only one animal sample by WJ $E_{80–10}$ application and none by WJ $E_{60–10}$ injection, which is another remarkable difference to the high incidence of cell misplacement after transurethral needle injection. To sum up, by WJ $E_{80–10}$ injection, the advantage of precise delivery of cell more evenly in the tissue targeted and closely to urethral sphincter muscle must be balanced with the disadvantage of an elevated risk of full penetration and tissue damage.

In this research project, only double injection in the lateral sites of the urethra of each animals were explored. Given the considerable low impact by WJ $E_{60–10}$ both, in cadaveric samples and in vivo, we supposed that by more injection points by WJ $E6_{0–10}$ injection, like 4 times injections at 2, 5, 8, 11 o'clock directions, could even improve the cell distribution without elevated risks of full penetrations as recorded by the unsuspected side effect using the WJ $E_{80–10}$ protocol in the pigs. Alternatively, there may be a chance to adjust the injection protocol and to generate e.g., pressure profiles at WJ $E_{60–60–10}$, a repeated tissue penetration injection with injection fluid only at the same site, which could open more space without any damage to muscle layer and to transport by that more cells closer to sphincter muscle. Moreover, modification of the duration and injection volumes of the two pressure phase may be also a key for deeper and wider cell delivery. These hypotheses would be part in our future experiments. In this study, we try to stick as much as possible to the control parameters published recently to facilitate a comparison of the outcome of the 3 animal groups investigated here and animals investigated recently[53]. Even like this, the experimental groups could only be compared pairwise.

In our experiment, it was our main goal investigate the possibility of MDC injection by WJ in the porcine urethral sphincter in vitro and in vivo and to demonstrate viability of cells injected. This study therefore was designed to pave way for future experiments in the context of prevention of urinary incontinence by restoring the

physiological function of the urethra through skeletal muscle regeneration by cell injection. The regeneration is a highly coordinated process including the strict regulation of multiple cellular and molecular responses. Beneath each layer of skeletal muscle there are satellite cells, which are usually keep in a resting state[81]. In response to certain stimuli, they restart the cell cycle and differentiate into MPCs, which are part of the myogenic lineage. Therefore, the myoblast seemed the most suitable and accessible cell source for muscle engineering. All the pMDCs employed in this study were analysed for the expression of specific myogenic markers by either qPCR of cDNA or by immunofluorescence. The expression of porcine desmin ("Schwein"−Desmin; sDesmin) which is a marker for muscle tissue in embryogenesis, was determined in the cells prepared. As myogenic progenitor marker as well as the quiescent activation marker sMyf5 and myogenic basic helix−loop−helix transcription factor sMyoD1, which play important roles in myoblasts differentiation were detected[82]. sMSTN normally limits the skeletal muscle mass as a natural inhibitor of muscle growth and development[83]. The lower expression of sMSTN in the newborn t.g. boar group compared to the adult WT group indicated that both of the two MDCs have stronger proliferation potential ability than newborn wildtype pig, which may become more effective and efficient MDCs populations for next level of SUI study. Expression of fast−twitch myosin and its gene Myl1 implied that these cells may match the phenotype of fast−twitch muscles cells of the urethral closure complex[84]. The slow myosin was undetectable in all groups investigated. This may be due to the fact that it is expressed only in mature slow−twitch myofibers but not in myoblasts[85]. However, as Jing−hua reported, Myh7 was activated in a subpopulation of myoblasts and co−expressed with Pax7. But this did not restrict the differentiation to slow myotubes[86]. But precise analyses of individual subsets of the pMDCs phenotypes of cells employed in my thesis is not the main focus of this study. In total, three cell pMDC

characterized cell populations prepared and used for injections in cadaveric urethra samples or for in vivo experiments. In addition and as mentioned above, in our study cells from 5–7 day old male pigs were isolated, expanded and injected into the urethra of female littermates to provide a homologous source of transplanted cells but to avoid immune response interference with the results of the experiments.

Retrieving injected cells from living animals immediately after injection is technically challenging and was not approved by the Animal Authorities. As alternative we investigated if cellular nuclei and somata appeared intact in the micrographs from frozen sections of tissue samples after 1, 3, and 7 days of follow−up. Round defined DAPI−stained nuclei surrounded by a defined fluorescence were considered as a first indicator on an intact cell. To verify that injected cells remained intact after WJ injection, the pSRY gene were detected by PCR in all samples in this in vivo study. Although this end−point PCR could not quantify the number of intact cells, the injected male cells contained sufficiently amounts of intact Y−chromosome in the urethra samples after either WJ $E_{80–10}$ or $E_{60–10}$ injection, and harvested after incubation times ranging from a few hours, i.e., day 1 to 7 days follow−up. Necrosis of injected cells or tissue were not detected in the cryosection samples neither by HE nor by Azan staining. Furthermore, the injected cells were identified more easily upon Azan staining than by HE in every group, which indicated that Azan could be more suitable for tracing the injected cells and the whole tissue structure.

5 Summary

5.1 Summary in English

Stress urinary incontinence is the most common type of urinary incontinence. It reduces the quality of life of patients. Actual standard surgical therapeutic modalities are offering a symptomatic relief without treating the underlying disorder. Therefore, we developed a novel cell injection technology to deliver viable cells for recovery of the function of the urethral sphincter by WaterJet (WJ, ERBE). Here we investigated if a) porcine muscle−derived cells (pMDC) could be injected by WJ in both, cadaveric samples and living porcine urethra with high viability, b) the WJ inherits the risk of full tissue penetration of the porcine urethra and thus loss of cells, and c) WJ grants improved precision of cell injection and distribution in tissues targeted.

The pMDC were produced from male boars and characterized by qRT−PCR and immunofluorescence. Visualized by Calcein AM vs EthD−1, cells were injected into cadaveric porcine urethral by WaterJet vs William's Needle. In another in vivo study, cells labelled with PKH 26 or/and BacMam, were injected in living female pigs by WaterJet using either a moderate ($E_{60–10}$; n = 18) or elevated pressure ($E^{80–10}$; n = 6) protocol, and follow-up (f/u) of up to 7 days. Cell injections targeted the site of the maximum urethral closure pressure (Aquarius TT, Laborie Medical). After harvesting the whole bladder and urethra, cells were traced by an In Vivo Imaging System (IVIS, PerkinElmer) and visualized by fluorescence microscopy of cryosections. Nuclei were stained by DAPI, muscular tissue by phalloidin-iFluor 488. The pSRY gene was detected by PCR. The distribution of injected pMDC was measured as X−depth, Y−width, Z−height and calculated areas in the XY-, YZ-,

XZ- planes were analysed. The distance between sphincter muscle and injected cells (DISIC) was measured simultaneously.

The analyses provided experimental evidence that pMDCs injected by WaterJet in vitro were viable. Our in vivo study supported that cells appeared defined cellular somata with distinct nuclei and contained intact chromosomal DNA. The success rates of WJ cell application in living animals were significantly higher (≥ 95%, n = 24) when compared to needle injections. Only one out of six samples with full penetration was observed in the WJ $E_{80–10}$ group. The analyses of the 3D distribution of cells after WJ injection documented that the Y−width of the WJ E_{80-10} group was statistically significant wider ($P = 0.0479$) than that of WJ E_{60-10} group. The same was recorded for the cell distribution in Z-height ($P < 0.0001$). The YZ-plane of the WJ $E_{80–10}$ group was statistically significant larger ($P = 0.0005$) than that of WJ E_{60-10} group, as well as XZ-plane ($P = 0.0204$). The injection depth of WJ E_{80-10} compared to WJ E_{60-10} showed a statistically significant decrease in length ($P < 0.0001$). This indicated that WJ E_{80-10} injections transported cells closer to the targeted rhabdosphincter, but at a higher risk for full penetration.

We conclude that the novel WJ is a fast, precise, and easy-to-use innovative method to inject living cells in tissues with a significantly wider and diffuse distribution, with less disintegration of the tissue targeted, and at higher success rates.

5.2 Zusammenfassung

Die Belastungsinkontinenz ist die häufigste Form der Harninkontinenz. Sie reduziert die Lebensqualität der Patienten und Patientinnen deutlich. Die aktuell verwendeten chirurgischen Therapiemodalitäten bieten meist nur eine symptomatische Linderung, ohne die zugrunde liegende Störung zu behandeln. Daher haben wir eine neuartige Zellinjektionstechnologie entwickelt, um lebensfähige Zellen für die Wiederherstellung der Funktion des Harnröhrenschließmuskels durch WaterJet (WJ, ERBE) zu ermöglichen. Im Rahmen dieser Arbeit untersuchten wir, ob a) aus Schweinemuskeln stammende Zellen (pMDC) durch Nadelinjktion mit einer Williamsnadel (WN) sowohl in Kadaverproben als auch in die Harnröhre lebender Schweine mit hoher Lebensfähigkeit injiziert werden könnten, b) Injektionen per WJ das Risiko einer vollständigen Gewebedurchdringung der Schweineharnröhre und damit des Verlusts von Zellen birgt, und c) WJ Injektionen eine verbesserte Genauigkeit der Zellinjektion und -verteilung in Zielgeweben ermöglichen.

Die pMDC wurden von männlichen Ebern produziert und durch qRT-PCR und Immunfluoreszenz charakterisiert. Durch Calcein AM vs. EthD−1, wurden Zellen als vital charakterisiert und mittels WaterJet vs. Williams Needle in die Harnröhre von Schlachtschweinen injiziert. In einer anderen in-vivo-Studie wurden Zellen, die mit PKH 26 oder/und BacMam markiert waren, in lebende weibliche Schweine mit WaterJet injiziert, wobei entweder ein mäßiges (E60-10; n = 18) oder erhöhtes Druckprotokoll (E80-10; n = 6) verwendet, und Nachuntersuchungszeiträume von bis zu 7 Tagen realisiert wurden. Zellinjektionen zielten auf die Stelle des maximalen Harnröhrenverschlussdrucks, der mittels Urodynamik bestimmt wurde (Aquarius TT, Laborie Medical). Nach Entnahme der gesamten Blase und Harnröhre wurden die Zellen durch ein in-vivo-Bildgebungssystem (IVIS, PerkinElmer) im Gewebe lokalisiert und durch Fluoreszenzmikroskopie von

Kryoschnitten sichtbar gemacht. Kerne wurden mit DAPI, Muskelgewebe mit Phalloidin-iFluor 488 gefärbt. Das pSRY-Gen wurde durch PCR nachgewiesen. Die Verteilung von injiziertem pMDC wurde als X-Tiefe, Y-Breite, Z-Höhe gemessen und berechnete Bereiche in den XY-, YZ-, XZ-Ebenen wurden analysiert. Der Abstand zwischen Schließmuskel und injizierten Zellen (DISIC) wurde gleichzeitig gemessen.

Die Analysen lieferten experimentelle Beweise dafür, dass pMDCs, die von WaterJet in vitro injiziert wurden, lebensfähig waren. Unsere in-vivo-Studie unterstützte die Hypothese, dass Zellen als definierte zelluläre Somata mit unterschiedlichen Kernen erschienen und intakte chromosomale DNA enthielten. Die Erfolgsraten der WJ-Zellapplikation bei lebenden Tieren waren signifikant höher ($\geq$ 95 %, n = 24) im Vergleich zu Nadelinjektionen. Nur eine von sechs Proben mit vollständiger Penetration wurde in der WJ E80-10-Gruppe beobachtet. Die Analysen der 3D-Verteilung von Zellen nach WJ-Injektion dokumentierten, dass die Y-Breite der WJ E80-10-Gruppe statistisch signifikant breiter war ($P = 0.0479$) als die der WJ E60-10-Gruppe. Dasselbe wurde für die Zellverteilung in Z-Höhe aufgezeichnet ($P < 0.0001$). Die YZ-Ebene der WJ E80-10-Gruppe war statistisch signifikant größer ($P = 0.0005$) als die der WJ E60-10-Gruppe sowie die XZ-Ebene ($P = 0.0204$). Die Injektionstiefe von WJ E80-10 im Vergleich zu WJ E60-10 zeigte eine statistisch signifikante Verringerung der Länge ($P < 0.0001$). Dies deutete darauf hin, dass WJ E80-10-Injektionen Zellen näher an den anvisierten Rhabdosphinkter transportierten, jedoch mit einem höheren Risiko für eine vollständige Penetration einhergingen.

Wir kommen zu dem Schluss, dass das neuartige WJ eine schnelle, präzise und einfach anzuwendende innovative Methode ist, um lebende Zellen in Gewebe mit einer deutlich breiteren und diffusen Verteilung, mit geringerer Desintegration des Zielgewebes und mit höheren Erfolgsraten zu injizieren.

6 Bibliography

[1] D'Ancona C., Haylen B., Oelke M., et al. *The International Continence Society (ICS) report on the terminology for adult male lower urinary tract and pelvic floor symptoms and dysfunction.* Neurourol Urodyn, 2019. **38**(2): p. 433-477.

[2] Minassian V.A., Stewart W.F. and Wood G.C. *Urinary incontinence in women: variation in prevalence estimates and risk factors.* Obstet Gynecol, 2008. **111**(2 Pt 1): p. 324-31.

[3] Lukacz E.S., Santiago-Lastra Y., Albo M.E., et al. *Urinary Incontinence in Women: A Review.* Jama, 2017. **318**(16): p. 1592-1604.

[4] Melville J.L., Fan M.Y., Rau H., et al. *Major depression and urinary incontinence in women: temporal associations in an epidemiologic sample.* Am J Obstet Gynecol, 2009. **201**(5): p. 490.e1-7.

[5] Nam R.K., Herschorn S., Loblaw D.A., et al. *Population based study of long-term rates of surgery for urinary incontinence after radical prostatectomy for prostate cancer.* J Urol, 2012. **188**(2): p. 502-6.

[6] Zhang L., Zhu L., Xu T., et al. *A Population-based Survey of the Prevalence, Potential Risk Factors, and Symptom-specific Bother of Lower Urinary Tract Symptoms in Adult Chinese Women.* Eur Urol, 2015. **68**(1): p. 97-112.

[7] DuBeau C.E., Kuchel G.A., Johnson T., 2nd, et al. *Incontinence in the frail elderly: report from the 4th International Consultation on Incontinence.* Neurourol Urodyn, 2010. **29**(1): p. 165-78.

[8] Hunskaar S., Burgio K., Diokno A., et al. *Epidemiology and natural history of urinary incontinence in women.* Urology, 2003. **62**(4 Suppl 1): p. 16-23.

[9] Irwin G.M. *Urinary Incontinence.* Prim Care, 2019. **46**(2): p. 233-242.

[10] Kinchen K.S., Bump R.C. and Gobier J.R. *Prevalence and frequency of stress urinary incontinence among community-dwelling women.* European Urology Supplements, 2002. **1**(1): p. 85.

[11] Jung J., Ahn H.K. and Huh Y. *Clinical and functional anatomy of the urethral sphincter.* Int Neurourol J, 2012. **16**(3): p. 102-6.

[12] Zini L., Lecoeur C., Swieb S., et al. *The striated urethral sphincter of the pig shows morphological and functional characteristics essential for the evaluation of treatments for sphincter insufficiency.* J Urol, 2006. **176**(6 Pt 1): p. 2729-35.

[13] Hajebrahimi S., Azaripour A. and Sadeghi-Bazargani H. *Clinical and transperineal ultrasound findings in females with stress urinary incontinence versus normal controls.* Pak J Biol Sci, 2009. **12**(21): p. 1434-7.

[14] Reynolds W.S., Dmochowski R.R. and Penson D.F. *Epidemiology of stress urinary incontinence in women.* Curr Urol Rep, 2011. **12**(5): p. 370-6.

[15] Fonti Y., Giordano R., Cacciatore A., et al. *Post partum pelvic floor changes.* J Prenat Med, 2009. **3**(4): p. 57-9.

[16] Nygaard I.E. and Heit M. *Stress urinary incontinence.* Obstet Gynecol, 2004. **104**(3): p. 607-20.

[17] Kegel A.H. *Progressive resistance exercise in the functional restoration of the perineal muscles.* Am J Obstet Gynecol, 1948. **56**(2): p. 238-48.

[18] Dumoulin C., Cacciari L.P. and Hay-Smith E.J.C. *Pelvic floor muscle training versus no treatment, or inactive control treatments, for urinary incontinence in women.* Cochrane Database Syst Rev, 2018. **10**(10): p. Cd005654.

[19] Bo K. *Pelvic floor muscle exercise for the treatment of stress urinary incontinence: An exercise physiology perspective.* International Urogynecology Journal, 1995. **6**(5): p. 282-291.

[20] Morkved S. and Bo K. *Effect of postpartum pelvic floor muscle training in prevention and treatment of urinary incontinence: a one-year follow up.* Bjog, 2000. **107**(8): p. 1022-8.

[21] Ashworth P.D. and Hagan M.J.P. *Some Social Consequences of Non-compliance with Pelvic Floor Exercises.* 1993. **79**: p. 465-471.

[22] Burns P.A., Pranikoff K., Nochajski T.H., et al. *A comparison of effectiveness of biofeedback and pelvic muscle exercise treatment of stress incontinence in older community-dwelling women.* J Gerontol, 1993. **48**(4): p. M167-74.

[23] Moroni R.M., Magnani P.S., Haddad J.M., et al. *Conservative Treatment of Stress Urinary Incontinence: A Systematic Review with Meta-analysis of Randomized Controlled Trials.* Rev Bras Ginecol Obstet, 2016. **38**(2): p. 97-111.

[24] Javanbakht M., Moloney E., Brazzelli M., et al. *Economic evaluation of surgical treatments for women with stress urinary incontinence: a cost-utility and value of information analysis.* BMJ Open, 2020. **10**(6): p. e035555.

[25] Shamliyan T.A., Kane R.L., Wyman J., et al. *Systematic review: randomized, controlled trials of nonsurgical treatments for urinary incontinence in women.* Ann Intern Med, 2008. **148**(6): p. 459-73.

[26] Bezerra C.A. and Bruschini H. *Suburethral sling operations for urinary incontinence in women.* Cochrane Database Syst Rev, 2001(3): p. Cd001754.

[27] Lapitan M.C., Cody D.J. and Grant A.M. *Open retropubic colposuspension for urinary incontinence in women.* Cochrane Database Syst Rev, 2003(1): p. Cd002912.

[28] Vakalopoulos I., Kampantais S., Laskaridis L., et al. *New artificial urinary sphincter devices in the treatment of male iatrogenic incontinence.* Adv Urol, 2012. **2012**: p. 439372.

[29] Nambiar A.K., Bosch R., Cruz F., et al. *EAU Guidelines on Assessment and Nonsurgical Management of Urinary Incontinence.* Eur Urol, 2018. **73**(4): p. 596-609.

[30] Suarez O.A. and McCammon K.A. *The Artificial Urinary Sphincter in the Management of Incontinence.* Urology, 2016. **92**: p. 14-9.

[31] Cordon B.H., Singla N. and Singla A.K. *Artificial urinary sphincters for male stress urinary incontinence: current perspectives.* Med Devices (Auckl), 2016. **9**: p. 175-83.

[32] Gilchrist A.S. and Rovner E.S. *Managing complications of slings.* Curr Opin Urol, 2011. **21**(4): p. 291-6.

[33] Herschorn S. *Current status of injectable agents for female stress urinary incontinence.* Can J Urol, 2001. **8**(3): p. 1281-9.

[34] Burkhart K.S. *Urinary incontinence in women: assessment and management in the primary care setting.* Nurse Pract Forum, 2000. **11**(4): p. 192-204.

[35] Herrera-Imbroda B., Lara M.F., Izeta A., et al. *Stress urinary incontinence animal models as a tool to study cell-based regenerative therapies targeting the urethral sphincter.* Adv Drug Deliv Rev, 2015. **82-83**: p. 106-16.

[36] Bennington J., Williams J.K. and Andersson K.-E. *New concepts in regenerative medicine approaches to the treatment of female stress urinary incontinence.* Current Opinion in Urology, 2019. **29**(4).

[37] Yiou R., Mahrouf-Yorgov M., Trébeau C., et al. *Delivery of human mesenchymal adipose-derived stem cells restores multiple urological dysfunctions in a rat model mimicking radical prostatectomy damages through tissue-specific paracrine mechanisms.* Stem Cells, 2016. **34**(2): p. 392-404.

[38] Williams J.K., Dean A., Badlani G., et al. *Regenerative Medicine Therapies for Stress Urinary Incontinence.* J Urol, 2016. **196**(6): p. 1619-1626.

[39] Silwal Gautam S., Imamura T., Ishizuka O., et al. *Implantation of autologous adipose-derived cells reconstructs functional urethral sphincters in rabbit cryoinjured urethra.* Tissue Eng Part A, 2014. **20**(13-14): p. 1971-9.

[40] Cao B., Zheng B., Jankowski R.J., et al. *Muscle stem cells differentiate into haematopoietic lineages but retain myogenic potential.* Nat Cell Biol, 2003. **5**(7): p. 640-6.

[41] Lee J.Y., Qu-Petersen Z., Cao B., et al. *Clonal isolation of muscle-derived cells capable of enhancing muscle regeneration and bone healing.* J Cell Biol, 2000. **150**(5): p. 1085-100.

[42] Peng H. and Huard J. *Muscle-derived stem cells for musculoskeletal tissue regeneration and repair.* Transpl Immunol, 2004. **12**(3-4): p. 311-9.

[43] Hoshi A., Tamaki T., Tono K., et al. *Reconstruction of radical prostatectomy-induced urethral damage using skeletal muscle-derived multipotent stem cells.* Transplantation, 2008. **85**(11): p. 1617-24.

[44] Tamaki T., Uchiyama Y., Okada Y., et al. *Functional recovery of damaged skeletal muscle through synchronized vasculogenesis, myogenesis, and neurogenesis by muscle-derived stem cells.* Circulation, 2005. **112**(18): p. 2857-66.

[45] Furuta A., Carr L.K., Yoshimura N., et al. *Advances in the understanding of sress urinary incontinence and the promise of stem-cell therapy.* Rev Urol, 2007. **9**(3): p. 106-12.

[46] Lecoeur C., Swieb S., Zini L., et al. *Intraurethral transfer of satellite cells by myofiber implants results in the formation of innervated myotubes exerting tonic contractions.* J Urol, 2007. **178**(1): p. 332-7.

[47] Yiou R., Dreyfus P., Chopin D.K., et al. *Muscle precursor cell autografting in a murine model of urethral sphincter injury.* BJU Int, 2002. **89**(3): p. 298-302.

[48] Hart M.L., Izeta A., Herrera-Imbroda B., et al. *Cell Therapy for Stress Urinary Incontinence.* Tissue Eng Part B Rev, 2015. **21**(4): p. 365-76.

[49] Amend B., Kelp A., Vaegler M., et al. *Precise injection of human mesenchymal stromal cells in the urethral sphincter complex of Göttingen minipigs without unspecific bulking effects.* Neurourol Urodyn, 2017. **36**(7): p. 1723-1733.

[50] Burdzinska A., Dybowski B., Zarychta-Wiśniewska W., et al. *Limited accuracy of transurethral and periurethral intrasphincteric injections of cellular suspension.* Neurourol Urodyn, 2018. **37**(5): p. 1612-1622.

[51] Bennington J., Williams J.K. and Andersson K.E. *New concepts in regenerative medicine approaches to the treatment of female stress urinary incontinence.* Curr Opin Urol, 2019. **29**(4): p. 380-384.

[52] Jäger L., Linzenbold W., Fech A., et al. *A novel waterjet technology for transurethral cystoscopic injection of viable cells in the urethral sphincter complex.* Neurourol Urodyn, 2020. **39**(2): p. 594-602.

[53] Linzenbold W., Jäger L., Stoll H., et al. *Rapid and precise delivery of cells in the urethral sphincter complex by a novel needle-free waterjet technology.* BJU Int, 2021. **127**(4): p. 463-472.

[54] Li M., Cui T., Mills D.K., et al. *Comparison of selective attachment and growth of smooth muscle cells on gelatin- and fibronectin-coated micropatterns.* J Nanosci Nanotechnol, 2005. **5**(11): p. 1809-15.

[55] Metzger K., Tuchscherer A., Palin M.F., et al. *Establishment and validation of cell pools using primary muscle cells derived from satellite cells of pig skeletal muscle.* In Vitro Cell Dev Biol Anim, 2020. **56**(3): p. 193-199.

[56] *Cell and Tissue Culture: Laboratory Procedures in Biotechnology*. Culture Processes and Scale-Up, ed. Doyle A. and Griffiths J.B. 1998: WILEY.

[57] PERSAUD S.J. *Cell and tissue culture: laboratory procedures in biotechnology.* Cell Biochemistry and Function,, ed. Doyle A. and Griffiths J.B. Vol. 17. 1999: John Wiley & Sons Ltd.

[58] Quertermous T. *Size Fractionation Using Agarose Gels.* Current Protocols in Molecular Biology, 1987. **00**(1): p. 5.4.1-5.4.4.

[59] Hornbeck P. *Enzyme-Linked Immunosorbent Assays.* Current Protocols in Immunology, 1992. **1**(1): p. 2.1.1-2.1.22.

[60] Kelp A., Albrecht, Amend B., et al. *Comparing different diagnostic methods to evaluate stress urinary incontinence in large animal models [Abstracts]*, in *the 37th Congress of the Société Internationale d'Urologie*. 2017, World Journal of Urology: Centro de Congressos de Lisboa. p. 1-360.

[61] Osborn D.J., Dmochowski R.R., Harris C.J., et al. *Analysis of patient and technical factors associated with midurethral sling mesh exposure and perforation.* Int J Urol, 2014. **21**(11): p. 1167-70.

[62] Schimpf M.O., Rahn D.D., Wheeler T.L., et al. *Sling surgery for stress urinary incontinence in women: a systematic review and metaanalysis.* Am J Obstet Gynecol, 2014. **211**(1): p. 71.e1-71.e27.

[63] Aragón I.M., Imbroda B.H. and Lara M.F. *Cell Therapy Clinical Trials for Stress Urinary Incontinence: Current Status and Perspectives.* Int J Med Sci, 2018. **15**(3): p. 195-204.

[64] Hillary C.J., Roman S., MacNeil S., et al. *Regenerative medicine and injection therapies in stress urinary incontinence.* Nat Rev Urol, 2020. **17**(3): p. 151-161.

[65] Vilsbøll A.W., Mouritsen J.M., Jensen L.P., et al. *Cell-based therapy for the treatment of female stress urinary incontinence: an early cost-effectiveness analysis.* Regen Med, 2018. **13**(3): p. 321-330.

[66] Zhou S., Zhang K., Atala A., et al. *Stem Cell Therapy for Treatment of Stress Urinary Incontinence: The Current Status and Challenges.* Stem Cells Int, 2016. **2016**: p. 7060975.

[67] Yokoyama T., Yoshimura N., Dhir R., et al. *Persistence and survival of autologous muscle derived cells versus bovine collagen as potential treatment of stress urinary incontinence.* J Urol, 2001. **165**(1): p. 271-6.

[68] Yasuda T., Weisel R.D., Kiani C., et al. *Quantitative analysis of survival of transplanted smooth muscle cells with real-time polymerase chain reaction.* J Thorac Cardiovasc Surg, 2005. **129**(4): p. 904-11.

[69] Marquardt L.M. and Heilshorn S.C. *Design of Injectable Materials to Improve Stem Cell Transplantation.* Curr Stem Cell Rep, 2016. **2**(3): p. 207-220.

[70] Habib M., Shapira-Schweitzer K., Caspi O., et al. *A combined cell therapy and in-situ tissue-engineering approach for myocardial repair.* Biomaterials, 2011. **32**(30): p. 7514-23.

[71] Hashemzadeh M.R., Taghavizadeh Yazdi M.E., Amiri M.S., et al. *Stem cell therapy in the heart: Biomaterials as a key route.* Tissue Cell, 2021. **71**: p. 101504.

[72] Schmid F.A., Gascho D., Zoelch N., et al. *Feasibility, technique and accuracy of ultrasound-guided transurethral injections into the urinary sphincter of female cadavers: proof of concept.* BMC Urol, 2020. **20**(1): p. 167.

[73] Amer M.H., White L.J. and Shakesheff K.M. *The effect of injection using narrow-bore needles on mammalian cells: administration and formulation considerations for cell therapies.* J Pharm Pharmacol, 2015. **67**(5): p. 640-50.

[74] Schreiber J. *Investigation of the penetration depth of microparticles by water jet application in porcine urethra [German]*. [Thesis], 2020. Ph.D. Urology. Tübingen: Eberhard −Karls−Universität. Tuebingen, Germany.

[75] Beck F. *Penetration Depth and Distribution of Nanoparticles Sfter Injection into the Porcine Urethra Using a New Water Jet Technology.* [Thesis], 2020. Ph.D. Urology. Tübingen: Eberhard −Karls−Universität. Tuebingen, Germany.

[76] Enosawa S. and Kobayashi E. *Controllable Immunosuppression in Pigs as a Basis for Preclinical Studies on Human Cell Therapy.* Xenotransplantation, ed. S. M. 2020: IntechOpen.

[77] Castro R., Libânio D., Pita I., et al. *Solutions for submucosal injection: What to choose and how to do it.* World J Gastroenterol, 2019. **25**(7): p. 777-788.

[78] Jacques J., Kerever S., Carrier P., et al. *HybridKnife high-pressure glycerol jet injection for endoscopic submucosal dissection increases procedural ease and speed: a randomised study in pigs and a human case series.* Surg Endosc, 2016. **30**(7): p. 3152-9.

[79] Repici A., Maselli R., Carrara S., et al. *Standard needle versus needleless injection modality: animal study on different fluids for submucosal elevation.* Gastrointest Endosc, 2017. **86**(3): p. 553-558.

[80] Linzenbold W., Fech A., Hofmann M., et al. *Novel Techniques to Improve Precise Cell Injection.* Int J Mol Sci, 2021. **22**(12).

[81] Forcina L., Miano C., Pelosi L., et al. *An Overview about the Biology of Skeletal Muscle Satellite Cells.* Curr Genomics, 2019. **20**(1): p. 24-37.

[82] Hart M.L., Neumayer K.M., Vaegler M., et al. *Cell-based therapy for the deficient urinary sphincter.* Curr Urol Rep, 2013. **14**(5): p. 476-87.

[83] Xu K., Zhou H., Han C., et al. *Transcriptomic Analysis of MSTN Knockout in the Early Differentiation of Chicken Fetal Myoblasts.* Genes (Basel), 2021. **13**(1).

[84] Koraitim M.M. *The male urethral sphincter complex revisited: an anatomical concept and its physiological correlate.* J Urol, 2008. **179**(5): p. 1683-9.

[85] Chen J. and Wang D.Z. *microRNAs in cardiovascular development.* J Mol Cell Cardiol, 2012. **52**(5): p. 949-57.

[86] Wang J.H., Wang Q.J., Wang C., et al. *Heterogeneous activation of a slow myosin gene in proliferating myoblasts and differentiated single myofibers.* Dev Biol, 2015. **402**(1): p. 72-80.

7 Declaration

I would like to emphasize here that all my experimental works in this thesis were completed in the Laboratory of the Department of Urology of the University Tuebingen Hospital (UKT) at the Centre for Medical Research (ZMF) under the supervision of Prof. Dr. rer. nat. Wilhelm K. Aicher.

This project was designed and supported by Prof. Aicher. Most of the experiments were carried out independently by myself. Other contributions include: The development of WaterJet from Prof. Dr. Markus D. Enderle and Dr. Walter Linzenbold. The cell production, quality management, animal study and evaluation of data was supported in part by Dr. Niklas Harland, Jasmin Knoll, Tanja Abruzzese, Coney Bock. Martin Schenk for the animal husbandry.

I claim that the manuscript of thesis was written all by myself.

8 Acknowledgement

First of all, I would like to take this opportunity to thank my supervisor Prof. Wilhelm K. Aicher, for not only offering the chance to study as MD at Tuebingen, but also his outstanding guidance during my whole doctoral period. The passion and energy of him always influence me to accomplish my research better.

Second, I give my thank to Dr. Niklas Harland for the help on animal surgery and the guide on organoids project.

Third, I would like to thank my colleagues Tanja, Conny, Jasmin for the help on cell culture & staining. Dr. Christine, Yi, Nizar, Paul, Johannes and Ingrid for all the assistance of my work and life.

Fourth, thanks to ERBE company for providing the waterjet prototype equipment−ERBE jet 2.

This project was supported in part by grants from the EU (MUS.I.C., #731377); the BMBF (Multimorb-INKO, # 13GW007); the DFG (PoTuS, #429049495); from the EU's Horizon 2020 program (iNanoBIT, # 760986); from the BMBF to the German Centre for Diabetes Research (DZD e.V., # 82DZD00802); Zukunftsfonds, FBN Dummerstorf and in part by institutional funds.

Moreover, my special thanks to Prof. Arnulf Stenzl for accepting me in this unit to accomplish my MD thesis.

I also thank to my friend Jing, Jibin, Bo, Linyan, Yi and Wei for sharing the wonderful time at Germany.

Lastly, a great thanks to my family. Without their support and love, I could not persist such a long time to complete my study.

Tübingen, 22.06.2022

9 Publications & Congress abstracts

9.1 Publications

1. **Geng R**, Knoll J, Harland N, et al. *Replacing Needle Injection by a Novel Waterjet Technology Grants Improved Muscle Cell Delivery in Target Tissues.* Cell Transplant. 2022;31:9636897221080943. doi:10.1177/09636897221080943.

2. **Geng R**, Harland N, Montes-Mojarro IA, et al. *CD24: A Marker for an Extended Expansion Potential of Urothelial Cancer Cell Organoids In Vitro?* Int J Mol Sci. 2022;23(10):5453. doi:10.3390/ijms23105453.

9.2 Congress abstracts

1. **Geng R.**, Knoll J., Harland N., et al. *A novel needle−free technology waterjet by improved delivery to transport muscle−derived cells to the urethral sphincter of living pigs.* Abstract PL (# 31412706966), TERMIS-EU convention 2022, Krakow, Poland.

2. **Geng R.**, Lipke N., Mayer Ch., et al. *Immunohistochemical evaluation of immune checkpoint antigens and stem cell markers on the early vs late passage organoids of urothelial carcinoma cells.* Abstract #AM22−2439, 37th Annual EAU Congress 2022, Amsterdam, Nederland.

3. **Geng R.,** Knoll J., Linzenbold W., et al. *Waterjet: a novel technology to inject cells in predetermined regions of the urethral sphincter for improved cell therapy of urinary incontinence.* Abstract P_BF22 # 73. 6th TERMIS World Congress 2021, Maastricht, Nederland.

4. **Geng R.**, Knoll J., Harland N., et al. *WaterJet: A novel needle-free injection technique for cell therapy of stress urinary incontinence.* Abstract. Der Urologe. Suppl 1. 2021; V1 1.8. 73rd DGU Congress 2021, Stuttgart, Germany.